



Fermi National Accelerator Laboratory

ITP-SB-92-41
FERMILAB-Pub-92/271-T

$O(\alpha_s)$ Corrections to Heavy-Flavour Inclusive Distributions
in Electroproduction

E. LAENEN,

*Fermi National Accelerator Laboratory
P.O. Box 500, MS 106
Batavia, IL 60510, U.S.A.*

S. RIEMERSMA, J. SMITH

*Institute for Theoretical Physics,
State University of New York at Stony Brook,
NY 11794-3840, U.S.A.*

and

W. L. VAN NEERVEN

*Instituut Lorentz,
University of Leiden,
P.O.B. 9506, 2300 RA, Leiden,
The Netherlands.*

October 1992

Abstract

We examine the $O(\alpha_s)$ corrections to inclusive heavy-flavour differential distributions in transverse momentum and rapidity in electroproduction. We assume that the electron is tagged and present results for fixed x and Q^2 for c -quark production at HERA.



1 Introduction

Inclusive neutral-current heavy-flavour production

$$e^-(l_1) + P(p) \rightarrow e^-(l_2) + Q(p_1)(\bar{Q}(p_2)) + X, \quad (1.1)$$

at the eP collider HERA has been analysed within the framework of perturbative QCD [1] (X denotes the hadrons in the final state which are not detected). The dominant contribution to the cross section comes from the photon-gluon fusion reaction

$$\gamma(q) + g(k_1) \rightarrow Q(p_1) + \bar{Q}(p_2). \quad (1.2)$$

where $\gamma(q)$ is a spacelike virtual photon and $g(k_1)$ is an on-mass-shell gluon. Therefore a measurement of the inclusive production cross section provides an opportunity to determine the gluon density in the proton $g_p(\xi, M^2)$ at small momentum fraction ξ [2] (defined by the identity $k_1 \equiv \xi p$) and mass factorization scale M^2 . The $O(\alpha_S)$ corrections to the inclusive cross sections and inclusive heavy-quark distributions in transverse momentum (p_t) and rapidity (y) were discussed for a real photon ($q^2 = 0$) in [3] (see also [4]). These corrections are valid in the "no-tag" situation where the electron remains in the beam pipe and the Weizsäcker-Williams approximation is valid. Unfortunately the presence of a poorly determined hadronic (resolved) gluon density in the real photon $g_\gamma(x_\gamma, M^2)$ complicates the extraction of the gluon density in the proton $g_p(\xi, M^2)$ [5].

A more reliable test of QCD can be made for heavy-quark production cross sections and inclusive distributions when $Q^2 = -q^2 > 0$ (say $Q^2 \geq 2$ (GeV/c)²) because the magnitude of the resolved component in the virtual photon decreases as Q^2 increases. In this case the electron is tagged so its Bjorken scaling variable $x = Q^2/2p \cdot q$ and Q^2 values are known. At HERA the outgoing electron can be detected if $Q^2 \geq 4$ (GeV/c)². A measurement of the heavy-quark inclusive cross section then requires the analysis of a five-fold differential involving the heavy-quark energy and polar angle together with the azimuthal angle between the plane containing the incoming and the outgoing leptons and the plane containing the proton and the heavy quark, as well as x and Q^2 for the detected electron. We recently calculated the QCD corrections to the four-dimensional-differential cross section [6], having

integrated over the azimuthal angle. This involved the calculation of the bremsstrahlung process

$$\gamma^*(q) + g(k_1) \rightarrow Q(p_1) + \bar{Q}(p_2) + g(k_2), \quad (1.3)$$

and the virtual (one-loop) corrections to the reaction (1.2). Furthermore at $O(\alpha_S^2)$ we encounter a new production mechanism given by the process

$$\gamma^*(q) + q(\bar{q})(k_1) \rightarrow Q(p_1) + \bar{Q}(p_2) + q(\bar{q})(k_2). \quad (1.4)$$

The resulting partonic cross sections were determined in the $\overline{\text{MS}}$ scheme both for coupling constant renormalization as well as for mass factorization, which was also performed in the DIS scheme. As an application we computed in [6] the $O(\alpha_S)$ corrections to the heavy-flavour contributions to deep-inelastic structure functions, denoted by $F_2(x, Q^2, m^2)$ and $F_L(x, Q^2, m^2)$, where m is the heavy-flavour mass. To illustrate the effect of the higher-order corrections we adopted the Morfin-Tung (MT) parametrization of the parton densities presented in table I_4 (Fit B_1) of [7] with $\Lambda_4 = 0.194$ GeV/ c (in the $\overline{\text{MS}}$ scheme). Furthermore, we chose the renormalization scale (μ) to be equal to the mass factorization scale (M), so that $\mu^2 = M^2 = Q^2 + 4m_c^2$ and $\mu^2 = M^2 = Q^2 + m_b^2$ for c -quark and b -quark production respectively.

Our results showed that even for an inclusive measurement, the $O(\alpha_S)$ corrections to the deep-inelastic structure functions cannot be described by constant factors multiplying the Born cross section (commonly called K -factors). Indeed ratios such as

$$R_k(x, Q^2, m^2) = \frac{F_{k,g}^{(0)}(x, Q^2, m^2) + F_k^{(1)}(x, Q^2, m^2)}{F_{k,g}^{(0)}(x, Q^2, m^2)}, \quad (1.5)$$

($k = 2, L$) showed significant increases at small and large values of x at fixed Q^2 (see figs. 17a, 17b, 21a, and 21b in [6]). In this equation the superscript denotes the order in perturbation theory, (0) corresponding to the Born reaction (1.2), which is already $O(\alpha_S)$ and (1) to the $O(\alpha_S^2)$ terms given by the corrections to (1.2) and the contributions from (1.3) and (1.4). Combining the results in [6] with the $O(\alpha_S^2)$ corrections to the standard (massless-quark) structure functions $F_2(x, Q^2)$ and $F_L(x, Q^2)$ calculated in [8] we were able to make more quantitative statements about the heavy-quark contributions to the deep-inelastic structure functions [9]. Note that

we have analysed the QCD corrections to extrinsic heavy-flavour production and concentrated on the region of moderate and small x . The magnitude of an additional intrinsic component at large x has been investigated in [10].

In this article we discuss the corrections to the inclusive transverse momentum (p_t) and rapidity (y) distributions for heavy-quark production at fixed values of x and Q^2 . Since heavy quarks are detected by an analysis of their decay modes, information on the p_t and y distributions is crucial in any complete Monte Carlo program containing both heavy-quark production and decay. Programs presently available [1], [2] use only the Born approximation. It is therefore necessary to check whether the QCD corrections to these inclusive distributions can be accounted for by simple multiplicative factors or not, since, in addition to the choice of the scheme, there are now several scales to consider. For example M^2 can depend upon Q^2 , m^2 and p_t^2 . As it is impossible to cover all possible schemes and scales, our results should only be considered as an indication of the shapes of the corrections. Furthermore to reduce the number of plots we only present results for c -quark production since this has a larger cross section than that for b -quark production. Finally we choose the same schemes and scales as in [6], except for the p_t -distribution for which we take $M^2 = Q^2 + 4(p_t^2 + m_c^2)$. Comments on other scale choices will be made in the text.

The variation in scale provides us with an estimate of how much the uncalculated higher order corrections change our $O(\alpha_s^2)$ results in the appropriate regions of phase space. If all invariants and scales are roughly equal then there should not be any large logarithmic terms which destroy the reliability of the perturbation series expansion. Although the calculation in [6] is applicable to any eP collider, the results we present here are for x and Q^2 values relevant to HERA. Note that the details of the QCD correction calculation are available in [6] so we limit ourselves to a brief listing of the important definitions in the next section and then present our results. Some useful kinematic relations are given in the Appendix.

2 Inclusive Heavy-Quark Distributions

After performing the integration over the azimuthal angle the deep-inelastic-electroproduction cross section can be written as a four-dimensional-differential cross section in the form

$$\frac{d^4\sigma(S, T_1, U_1, x, z)}{dx dz dT_1 dU_1} = \frac{\alpha}{2\pi} \frac{1}{xz} \left[2(1-z) \frac{d^2\sigma_L(S, T_1, U_1, Q^2)}{dT_1 dU_1} + [1 + (1-z)^2] \frac{d^2\sigma_T(S, T_1, U_1, Q^2)}{dT_1 dU_1} \right], \quad (2.1)$$

where x and z denote the usual Bjorken scaling variables

$$x = \frac{Q^2}{2p \cdot q} \quad , \quad z = \frac{p \cdot q}{p \cdot l_1}, \quad (2.2)$$

related by $Q^2 = xz\bar{S}$ where $\bar{S} = (l_1 + p)^2$ and $\sqrt{\bar{S}} = 314$ GeV at HERA. The fine structure constant is $\alpha = e^2/4\pi$. The longitudinal- and transverse-virtual-photon cross sections occurring in (2.1) are denoted by $d\sigma_L$ and $d\sigma_T$ respectively. Both cross sections also depend on the heavy-flavour mass denoted by m . The other kinematic invariants which appear in the above cross section are defined by

$$\begin{aligned} S &= (p + q)^2 \quad , \quad S' = S + Q^2, \\ T_1 &= T - m^2 = (p - p_2)^2 - m^2 \quad , \\ U_1 &= U - m^2 = (q - p_2)^2 - m^2 \quad . \end{aligned} \quad (2.3)$$

Here $\sqrt{\bar{S}}$ stands for the c.m. energy of the virtual-photon-proton system. Further T and U are the squares of the momentum transfers between the outgoing heavy antiquark and the proton and virtual photon respectively (see fig.1 in [6]). If the heavy quark is detected, p_2 in (2.3) is replaced by p_1 .

In the figures discussed below we will plot the inclusive distributions $dF_k(x, Q^2, m^2, p_t)/dp_t$ and $dF_k(x, Q^2, m^2, y)/dy$ with $k = 2, L$. Here p_t and y denote the transverse momentum and rapidity in the c.m. frame of the photon-hadron system. These distributions can be derived from the longitudinal and transverse photon-hadron cross sections in (2.1). Let us define

$$\frac{d^2\sigma_L(S, T_1, U_1, Q^2)}{dT_1 dU_1} = \frac{4\pi^2\alpha}{Q^2} \frac{d^2F_L(x, Q^2, T_1, U_1)}{dT_1 dU_1}, \quad (2.4)$$

and

$$\frac{d^2\sigma_T(S, T_1, U_1, Q^2)}{dT_1 dU_1} = \frac{4\pi^2\alpha}{p \cdot q} \frac{d^2F_1(x, Q^2, T_1, U_1)}{dT_1 dU_1}. \quad (2.5)$$

Here we will concentrate on $d^2F_L/dT_1 dU_1$ and $d^2F_2/dT_1 dU_1$ where the latter is given by

$$\frac{d^2F_2(x, Q^2, T_1, U_1)}{dT_1 dU_1} = 2x \frac{d^2F_1(x, Q^2, T_1, U_1)}{dT_1 dU_1} + \frac{d^2F_L(x, Q^2, T_1, U_1)}{dT_1 dU_1}. \quad (2.6)$$

Note that when the above expressions are integrated over T_1 and U_1 we obtain the heavy-flavour contribution to the structure functions $F_k(x, Q^2, m^2)$ as presented in [6]. The longitudinal and transverse photon-hadron cross sections are obtained from their partonic analogues via the formula

$$S'^2 \frac{d^2\sigma_k(S, T_1, U_1, Q^2)}{dT_1 dU_1} = \sum_i \int_{\xi_{1-}}^1 \frac{d\xi}{\xi} f_i(\xi, M^2) s'^2 \frac{d^2\hat{\sigma}_{k,i}(s, t_1, u_1, Q^2, M^2)}{dt_1 du_1}, \quad (2.7)$$

where $d\hat{\sigma}_k(k = 2, L)$ are the reduced parton cross sections (Wilson coefficients) calculated in [6]. The kinematical variables s, s', t_1 and u_1 are defined in an analogous way as in (2.3) where now p is replaced by the incoming parton momentum $k_1 = \xi p$. The $f_i(\xi, M^2)$ ($i = q, \bar{q}, g$) denote the parton densities as defined in [7], which like the $d\hat{\sigma}_{k,i}$ depend on the mass factorization scale M which is equal to the renormalization scale. Finally the lower boundary ξ_{1-} in (2.7) is given by

$$\xi_{1-} = \frac{-U_1}{S' + T_1}. \quad (2.8)$$

From $d^2F_k/dT_1 dU_1$ one can derive the experimentally relevant distributions $d^2F_k/dy dp_t$. We define positive rapidity to be in the direction of the virtual-photon. Since the transformation $(T_1, U_1) \rightarrow (y, p_t)$ is not relevant to the text we give some details in the Appendix. As mentioned in [6] the rapidity distribution of the heavy quark changes when the latter is replaced by the heavy antiquark. This is due to an asymmetry under $t_1 \leftrightarrow u_1$ in the parton cross sections $d^2\hat{\sigma}_{k,q}, d^2\hat{\sigma}_{k,\bar{q}}$ leading to $(d^2\sigma_{k,i})_{i\gamma \rightarrow Q} \neq (d^2\sigma_{k,i})_{i\gamma \rightarrow \bar{Q}}$ for $i = q, \bar{q}$. (see (3.37) and (3.38) in [6]), where we define

$$t_1 = (k_1 - p_2)^2 - m^2, u_1 = (q - p_2)^2 - m^2. \quad (2.9)$$

However the difference is numerically very small so that we only will plot the rapidity distribution of the heavy antiquark.

We now turn to results for the inclusive distributions $dF_k(x, Q^2, m^2, p_t)/dp_t$ and $dF_k(x, Q^2, m^2, y)/dy$ with $k = 2, L$. The variables x and Q^2 are chosen in the relevant kinematic range covered by HERA, so we take $Q^2 = 10 \text{ (GeV/c)}^2$ and vary x from 0.1 to 0.0001. We use the two-loop corrected running coupling constant α_S in the $\overline{\text{MS}}$ scheme with four light flavours. For the parton densities we choose the MT-B1 set presented in table I_4 of [7] with $\Lambda_4 = 0.194 \text{ GeV/c}$. In order to show the effect of the $O(\alpha_S)$ -corrections we write a series expansion in α_S for the deep-inelastic distributions in (2.4) and (2.5) where the $O(\alpha_S^{m+1})$ contribution is denoted by $dF_k^{(m)}$. Furthermore we distinguish between the initial-state gluon and initial-state-(anti)quark contribution to $dF_k^{(m)}$ by splitting $dF_k^{(m)}$ into $dF_{k,g}^{(m)}$ (1.3) and $dF_{k,q}^{(m)}$ ($dF_{k,\bar{q}}^{(m)}$) (1.4). Notice that the Born contribution is given by $dF_{2,g}^{(0)}$ corresponding to the process (1.2).

We begin with the p_t -distributions $dF_2(x, Q^2, m_c^2, p_t)/dp_t$ for c-quark production assuming the mass $m_c = 1.5 \text{ GeV/c}^2$ and $M^2 = Q^2 + 4m_c^2$. In this case we checked that the integrated distributions agree numerically with the values for the deep-inelastic structure functions $F_2(x, Q^2, m_c^2)$ given in [6]. We now change the mass factorization scale for the p_t -distributions to the more standard choice $M^2 = Q^2 + 4(p_t^2 + m_c^2)$. Figures 1-4 display the results for the mass factorization scale $M^2 = Q^2 + 4(p_t^2 + m_c^2)$, $Q^2 = 10 \text{ (GeV/c)}^2$, and $x = 0.1, 0.01, 0.001, \text{ and } 0.0001$ respectively.

From the figures we infer that the $O(\alpha_S)$ -correction denoted by $dF_2^{(1)}/dp_t$ is positive over the entire p_t -range when $x \geq 0.001$ (see figs.1,2,3). For $x = 0.0001$ it becomes negative in the small p_t region whereas it becomes positive again as p_t increases (see fig.4). Because showing the corrections to the p_t distribution on a semi-logarithmic scale distorts the actual size of the $O(\alpha_S)$ corrections, we illustrate the effects of this correction more effectively by plotting the ratio

$$R_k(x, Q^2, m_c^2, p_t) = \frac{dF_{k,g}^{(0)}(x, Q^2, m_c^2, p_t)/dp_t + dF_k^{(1)}(x, Q^2, m_c^2, p_t)/dp_t}{dF_{k,g}^{(0)}(x, Q^2, m_c^2, p_t)/dp_t}, \quad (2.10)$$

with $k = 2$ in fig.5.

Figure 5 reveals that as $x \rightarrow 0$, the corrections decrease relative to the Born contribution. It is important to note that $dF_2(x, Q^2, m_c^2, p_t)/dp_t$ is peaked around $p_t = m_c/2$, so the corrections to the integrated structure function $F_2(x, Q^2, m_c^2)$ are primarily from this region, and not the region of larger p_t , where $dF_2(x, Q^2, m_c^2, p_t)/dp_t$ is rapidly falling. In the region of small p_t , however, perturbation theory breaks down and one should apply resummation techniques as done in [11] or [12]. Note the result that the corrections decrease as $x \rightarrow 0$ could be anticipated from the magnitude of the integrated contribution given in fig.17a of [6]. In the case that x is small ($x \leq 0.001$) the correction rises in the small- p_t region and remains around the 50% level for $p_t \geq 5 \text{ GeV}/c$. Though we would see a steep rise as $p_t \rightarrow p_t^{max} = \sqrt{S/4 - m_c^2}$ if we had extended the plot to include these values of p_t , as we do for the larger values of x , this region does not contribute much to the integrated result due to the steeply falling spectrum.

One can understand the shape of these curves by investigating the individual contributions to $dF_2^{(1)}/dp_t$ which are given by $dF_{2,q}^{(1)}/dp_t$ (1.3) and $dF_{2,\bar{q}}^{(1)}/dp_t$ (1.4). For $x \geq 0.01$, $dF_{2,q}^{(1)}/dp_t$ is positive for all values of p_t . The γq correction $dF_{2,q}^{(1)}/dp_t$ is negative for small values of p_t and positive for large values of p_t for all x -values. Since the gluonic contribution is numerically more important at small p_t the result is that we find a positive correction. However for $x = 0.0001$ the gluonic correction is negative near the edges of phase space $p_t \rightarrow 0$ and $p_t \rightarrow p_t^{max} = \sqrt{S/4 - m_c^2}$. Also since the integrated result is dominated by the behaviour in the small p_t region the fact that fig.17a in [6] shows a small increase at $x = 0.0001$ is due to effects in both the gluon and the quark channels. Further it appears that for large p_t -values $|dF_{2,q}^{(1)}/dp_t| > |dF_{2,\bar{q}}^{(1)}/dp_t|$ whereas for small p_t -values $|dF_{2,q}^{(1)}/dp_t| < |dF_{2,\bar{q}}^{(1)}/dp_t|$. Both statements are generally true over the whole x -range. This is understandable for large x where the quark densities dominate over the gluon. However at small x this is due to the complicated structure of the reduced cross sections $d\hat{\sigma}_{2,i}$ ($i = q, \bar{q}, g$) in (2.7).

When we choose a p_t -independent scale such as $M^2 = Q^2 + 4m_c^2$, then the values for the $O(\alpha_S)$ -corrected p_t -distributions are increased roughly by a factor of two as p_t gets large. Furthermore we observe that the decrease of $R_2(x, Q^2, m_c^2, p_t)$ as a function of p_t takes place at much larger values of p_t than in the case of a p_t -dependent mass factorization scale. In view of this we conclude that the scale $M^2 = Q^2 + 4(p_t^2 + m_c^2)$ is a better choice than

$$M^2 = Q^2 + 4m_c^2.$$

In figs.6-9 we show the corresponding plots for $dF_L(x, Q^2, m_c^2, p_t)/dp_t$ with $M^2 = Q^2 + 4(p_t^2 + m_c^2)$. Comparing dF_L/dp_t with dF_2/dp_t we see that the peak in the distributions becomes much more conspicuous in the former than the one observed in the latter. This is due to the vanishing of dF_L/dp_t as $p_t \rightarrow 0$. However as one can infer from $R_L(x, Q^2, m_c^2, p_t)$ (2.10) in fig.10 the Born contribution $dF_{L,g}^{(0)}/dp_t$ vanishes much more quickly than $dF_{L,g}^{(1)}/dp_t$ as $p_t \rightarrow 0$, causing R_L to become large. For p_t -values in the area of the peak of dF_L/dp_t , the effect from $dF_{L,g}^{(1)}/dp_t$ as $x \rightarrow 0$ is decreasing and even becomes negative in a small region when $x = 0.0001$. Thus, the cancellation against $dF_{L,q}^{(1)}/dp_t$ is reduced and the dip in fig.10 becomes more pronounced. In the region of intermediate p_t , $dF_{L,g}^{(1)}/dp_t$ is still substantial relative to $dF_{L,g}^{(0)}/dp_t$, while $dF_{L,q}^{(1)}/dp_t$ is somewhat less important. For larger p_t , $dF_{L,g}^{(1)}/dp_t$ decreases and changes sign for $x \leq 0.0001$. On the other hand for large p_t , the distribution $dF_{L,q}^{(1)}/dp_t$ dominates all other contributions indicating the importance of the valence-quark densities in this region. Figure 10 reveals a large sensitivity of R_L to the chosen values for p_t except for $x = 0.001$ where the corrections are roughly constant when $p_t \geq 5$ GeV/c. However their large size (100%) is an indication of the poor convergence of the QCD perturbation series in regions of phase space where the longitudinal cross section in (2.1) cannot be neglected. In the analysis of the differential cross section note that dF_L/dp_t is usually numerically smaller than dF_2/dp_t . These findings are consistent with the results for the integrated distributions in fig.17b in [6]. Even though the corrections seem large at moderate p_t , the fact that the underlying spectrum is falling rapidly means that the integrated contributions are most sensitive to small p_t and therefore the corrections are moderate in the region $0.001 < x < 0.01$.

Next we investigate the rapidity distributions $dF_2(x, Q^2, m_c^2, y)/dy$ for c -quark production, with mass $m_c = 1.5$ GeV/c², but this time assuming the original mass scale $M^2 = Q^2 + 4m_c^2$ as in [6]. We fix $Q^2 = 10$ (GeV/c)² and vary x in decades from $x = 0.1$ to $x = 0.0001$ showing these results in figs.11-14. The correction $dF_{2,g}^{(1)}/dy$ is generally larger than the Born contribution $dF_{2,g}^{(0)}/dy$ in the negative rapidity range, becomes comparable in the central rapidity region, and dies off in the large positive rapidity range, where it eventually becomes negative. The contribution $dF_{2,g}^{(1)}/dy$ is responsible for

the bulk of the $O(\alpha_S)$ corrections as the contribution $dF_{2,q}^{(1)}/dy$ is generally an order of magnitude smaller and becomes mostly negative for large x . However at small x , it is mainly positive, turning negative only in the region of large positive rapidity. Again the semilogarithmic plots in figs.11-14 tend to distort the actual influence of the $O(\alpha_S)$ corrections. To demonstrate the higher-order effects more clearly, we define the ratio

$$R_k(x, Q^2, m_c^2, y) = \frac{dF_{k,g}^{(0)}(x, Q^2, m_c^2, y)/dy + dF_k^{(1)}(x, Q^2, m_c^2, y)/dy}{dF_{k,g}^{(0)}(x, Q^2, m_c^2, y)/dy}, \quad (2.11)$$

with $k = 2, L$, where $R_2(x, Q^2, m_c^2, y)$ is presented in fig.15. At large negative rapidity R_2 is very large. It decreases towards $y = 0$ where it becomes relatively flat and the corrections are reasonable. This flattening extends over a larger range in y when x gets smaller. In the large positive rapidity region R_2 drops off very rapidly and even becomes negative. This effect is primarily due to $dF_{2,g}^{(1)}/dy$ which becomes negative and its magnitude is larger than the Born contribution $dF_{2,g}^{(0)}/dy$. From the above we conclude that the corrections are generally stable in the central rapidity region and range numerically from 50% to 100%. Notice that the integrated distributions represented by the structure function $F_2(x, Q^2, m_c^2)$ receives its main support from the large positive rapidity region where the corrections are small. This explains why fig.15 is consistent with the integrated plot in fig.19a in [6].

In figs.16-19 we show the rapidity plots for $dF_L(x, Q^2, m^2, y)/dy$. In the regions of negative rapidity, $dF_{L,g}^{(1)}/dy$ dominates the Born contribution $dF_{L,g}^{(0)}/dy$, and as x becomes smaller, the difference is several orders of magnitude. Furthermore, $dF_{L,q}^{(1)}/dy$ makes a significant contribution relative to the Born in the same region. In the central rapidity region, $dF_{L,g}^{(1)}/dy$ is decreasing but still considerably larger than $dF_{L,g}^{(0)}/dy$. The contribution from the γq channel $dF_{L,q}^{(1)}/dy$ is still significant but decreasing as well. In the positive rapidity region, $dF_{L,q}^{(1)}/dy$ becomes negative, closer to the central rapidity region as x increases. The gluonic correction decreases as well, providing a reasonably moderate correction in the large positive rapidity region where dF_L/dp_t is peaked. As y^{max} is approached, both the γg and the γq corrections turn negative, however becoming positive again at the very edge of phase space and are responsible for the enormous rise in $R_L(x, Q^2, m_c^2, y)$ as $y \rightarrow y^{max}$.

Finally we remark that we have also computed the corrections for $Q^2 = 4$ $(\text{GeV}/c)^2$ and for $Q^2 = 100$ $(\text{GeV}/c)^2$ covering the same range in x . Although there are changes in the plots the overall picture remains the same so our conclusions are unaltered.

For completeness we have also plotted the p_t and y distributions for b -quark production using the parameters $m_b = 4.75$ GeV/c^2 , $Q^2 = 10$ $(\text{GeV}/c)^2$ and $M^2 = Q^2 + p_t^2 + m_b^2$, $M^2 = Q^2 + m_b^2$ respectively. While the results are similar to the case of the c -quark the corresponding plots to figs. 5,10,15 and 20 do indicate less sensitivity to the variation of M^2 .

We have reported here the first results on the $O(\alpha_s^2)$ QCD contributions to the inclusive heavy-flavour distributions at fixed values of the x and Q^2 of the electron. We have demonstrated that the higher order corrections to the inclusive heavy-quark p_t and y distributions are sensitive to the choice of the mass factorization and renormalization scales. Fortunately the integrated differential distributions for the dominant structure function $F_2(x, Q^2, m_c^2)$ show some stability in the region $0.0001 < x < 0.01$ which is consistent with moderate corrections to the inclusive p_t and y distributions near their respective maxima. Since actual experiments will have acceptance cuts it is not clear which region of x and Q^2 will be the most relevant. Therefore further work will be required to clarify the situation when experimental data become available.

While this work was under way we received a preprint [13] containing an examination of the electroproduction of heavy flavours at high energies including leading contributions at small x . These contributions originate from gluon exchanges in t -channel processes which are all positive. It turns out that these effects, when resummed, are very small in the HERA range. This approach is different from ours. We have calculated the exact corrections up to $O(\alpha_s^2)$ in perturbation theory, which implies that the coefficients in the perturbation series can become negative due to virtual corrections and mass factorization. These negative corrections never show up in the calculation of [13], and thus our results are quite different in the HERA regime.

Acknowledgements

The work in this paper was supported in part under the contracts NSF 92-11367 and DOE DE-AC02-76CHO3000. Financial support was also provided by the Netherlands Organization for Scientific Research (NWO) and the Texas National Research Laboratory Commission.

Appendix

The relationship between T_1 and U_1 , the heavy-quark transverse mass m_T , and the rapidity y in the c.m. frame of the virtual-photon-proton system is complicated when both Q^2 and m^2 are non-zero. Using the definitions in (2.3) the energy of the outgoing heavy antiquark is

$$\tilde{E} = \frac{-Q^2 - T_1 - U_1}{2\sqrt{S}}, \quad (\text{A.1})$$

where $Q^2 > 0$. The transverse mass is determined by

$$S'^2 m_T^2 = S' T_1 U_1 + Q^2 T_1^2 + Q^2 S' T_1, \quad (\text{A.2})$$

where $S' = S + Q^2$. The square of the longitudinal momentum is

$$\tilde{P}_L^2 = \tilde{E}^2 - m_T^2, \quad (\text{A.3})$$

so we define the rapidity to be

$$y = \frac{1}{2} \ln \left(\frac{\tilde{E} + \tilde{P}_L}{\tilde{E} - \tilde{P}_L} \right). \quad (\text{A.4})$$

After some algebra we find the relations

$$\begin{aligned} T_1 &= -\frac{S'}{\sqrt{S}} m_T e^y, \\ U_1 &= -Q^2 - m_T (S e^{-y} - Q^2 e^y) / \sqrt{S}. \end{aligned} \quad (\text{A.5})$$

The Jacobian of the change of variables from the two-dimensional integration over T_1 and U_1 to the corresponding integration over m_T^2 and y yields S' , so

$$\int d(-T_1) \int d(-U_1) = S' \int dm_T^2 \int dy \quad (\text{A.6})$$

where the integration limits are given by

$$\begin{aligned} \frac{S'}{2}(1 - \beta) &\leq -T_1 \leq \frac{S'}{2}(1 + \beta) \\ \frac{S'}{-T_1} \left(m^2 - \frac{T_1^2 Q^2}{S'^2} - \frac{Q^2 T_1}{S'} \right) &\leq -U_1 \leq S' + T_1 \\ m^2 &\leq m_T^2 \leq \frac{S}{4} \\ -\cosh^{-1} \left(\frac{\sqrt{S}}{2m_T} \right) &\leq y \leq \cosh^{-1} \left(\frac{\sqrt{S}}{2m_T} \right) \end{aligned} \quad (\text{A.7})$$

where $\beta = \sqrt{1 - 4m^2/S}$. Changing the order of integration, we get

$$\int d(-T_1) \int d(-U_1) = S' \int dy \int dm_T^2 \quad (\text{A.8})$$

with the corresponding change in the integration limits given by

$$\begin{aligned} -\frac{1}{2} \ln \left(\frac{1+\beta}{1-\beta} \right) &\leq y \leq \frac{1}{2} \ln \left(\frac{1+\beta}{1-\beta} \right) \\ m^2 &\leq m_T^2 \leq \frac{S}{4 \cosh^2(y)} \end{aligned} \quad (\text{A.9})$$

References

- [1] For a review of recent papers on this subject consult the article by A. Ali and D. Wyler in Proceedings of the Workshop Physics at HERA p.669 (1991) eds. W. Buchmüller and G. Ingelman.
- [2] R. van Woudenberg et al., in Proceedings of the Workshop Physics at HERA p.741 (1991) eds. W. Buchmüller and G. Ingelman.
- [3] J. Smith and W.L. van Neerven, Nucl.Phys. B374 (1992) 36.
- [4] R. K. Ellis and P. Nason, Nucl. Phys. B312 (1989) 551.
- [5] S. Riemersma, J. Smith, and W.L. van Neerven, Phys.Letts B282 (1992) 171.
- [6] E. Laenen, S. Riemersma, J. Smith, and W.L. van Neerven, ITP-SB-92-09 (May 1992), accepted for publication in Nucl.Phys.
- [7] J.G. Morfín and W-K. Tung, Z.Phys. C52, (1991) 13.
- [8] E.B. Zijlstra and W.L. van Neerven, INLO-PUB-1/92, accepted for publication in Nucl.Phys.; W.L. van Neerven and E.B. Zijlstra, Phys. Letts. B272 (1991) 127; E.B. Zijlstra and W.L. van Neerven, ibid B273 (1991) 476.
- [9] E. Laenen, S. Riemersma, J. Smith, and W.L. van Neerven, Phys. Letts. B291 (1992) 325.
- [10] S.J. Brodsky, P. Hoyer, A.H. Mueller and W-K.Tang, Nucl. Phys. B369(1992) 519.
- [11] E. Laenen, J. Smith, W.L. van Neerven, Nucl. Phys. B369 (1992) 543.
- [12] P.B. Arnold and R.P. Kauffman, Nucl.Phys.B349 (1991) 381.
- [13] G. Marchesini and B.R. Webber, CERN-TH.6595/92.

Fig.1. The inclusive differential distributions $dF_{2,g}^{(0)}(x, Q^2, m_c^2, p_t)/dp_t$ (solid curve) and the sum of $dF_{2,g}^{(0)}(x, Q^2, m_c^2, p_t)/dp_t + dF_2^{(1)}(x, Q^2, m_c^2, p_t)/dp_t$ (dashed curve) at $x = 0.1$ and $Q^2 = 10$ (GeV/c)².

Fig.2. Same as Fig.1 but for $x = 0.01$

Fig.3. Same as Fig.1 but for $x = 0.001$

Fig.4. Same as Fig.1 but for $x = 0.0001$

Fig.5. The p_t -dependences of $R_2(x, Q^2, m_c^2, p_t)$ at $Q^2 = 10$ (GeV/c)² and $x = 0.1$ (dot-dashed curve), 0.01 (long-dashed), 0.001 (short-dashed) and 0.0001 (solid) respectively.

Fig.6. The inclusive differential distributions $dF_{L,g}^{(0)}(x, Q^2, m_c^2, p_t)/dp_t$ (solid curve) and the sum of $dF_{L,g}^{(0)}(x, Q^2, m_c^2, p_t)/dp_t + dF_L^{(1)}(x, Q^2, m_c^2, p_t)/dp_t$ (dashed curve) at $x = 0.1$ and $Q^2 = 10$ (GeV/c)².

Fig.7. Same as Fig.6 but for $x = 0.01$

Fig.8. Same as Fig.6 but for $x = 0.001$

Fig.9. Same as Fig.6 but for $x = 0.0001$

Fig.10. The p_t -dependences of $R_L(x, Q^2, m_c^2, p_t)$ at $Q^2 = 10$ (GeV/c)² and $x = 0.1, 0.01, 0.001$ and 0.0001 respectively. The notation is the same as in fig.5.

Fig.11. The inclusive differential distributions $dF_{2,g}^{(0)}(x, Q^2, m_c^2, y)/dy$ (solid curve) and the sum of $dF_{2,g}^{(0)}(x, Q^2, m_c^2, y)/dy + dF_2^{(1)}(x, Q^2, m_c^2, y)/dy$ (dashed curve) at $x = 0.1$ and $Q^2 = 10$ (GeV/c)².

Fig.12. Same as Fig.11 but for $x = 0.01$

Fig.13. Same as Fig.11 but for $x = 0.001$

Fig.14. Same as Fig.11 but for $x = 0.0001$

Fig.15. The y -dependences of $R_2(x, Q^2, m_c^2, y)$ at $Q^2 = 10$ (GeV/c)² and $x = 0.1$ (dot-dashed curve), 0.01 (long-dashed), 0.001 (short-dashed) and 0.0001 (solid) respectively.

Fig.16. The inclusive differential distributions $dF_{L,g}^{(0)}(x, Q^2, m_c^2, y)/dy$ (solid curve) and the sum of $dF_{L,g}^{(0)}(x, Q^2, m_c^2, y)/dy + dF_L^{(1)}(x, Q^2, m_c^2, y)/dy$ (dashed curve) at $x = 0.1$ and $Q^2 = 10$ (GeV/c)².

Fig.17. Same as Fig.16 but for $x = 0.01$

Fig.18. Same as Fig.16 but for $x = 0.001$

Fig.19. Same as Fig.16 but for $x = 0.0001$

Fig.20. The y -dependences of $R_L(x, Q^2, m_c^2, y)$ at $Q^2 = 10$ (GeV/c)² and $x = 0.1, 0.01, 0.001$ and 0.0001 respectively. The notation is the same as in fig.15.

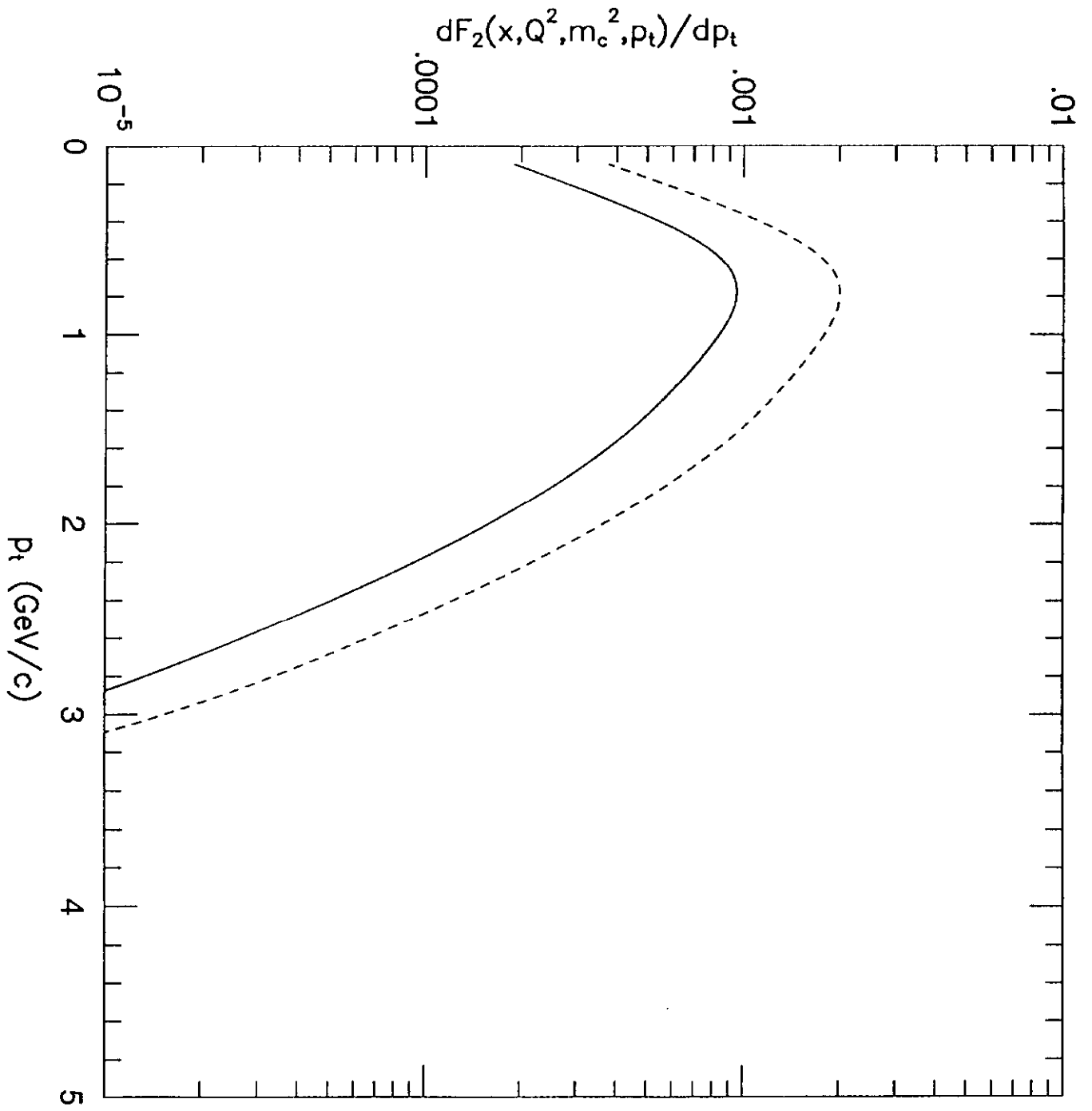


Fig. 1

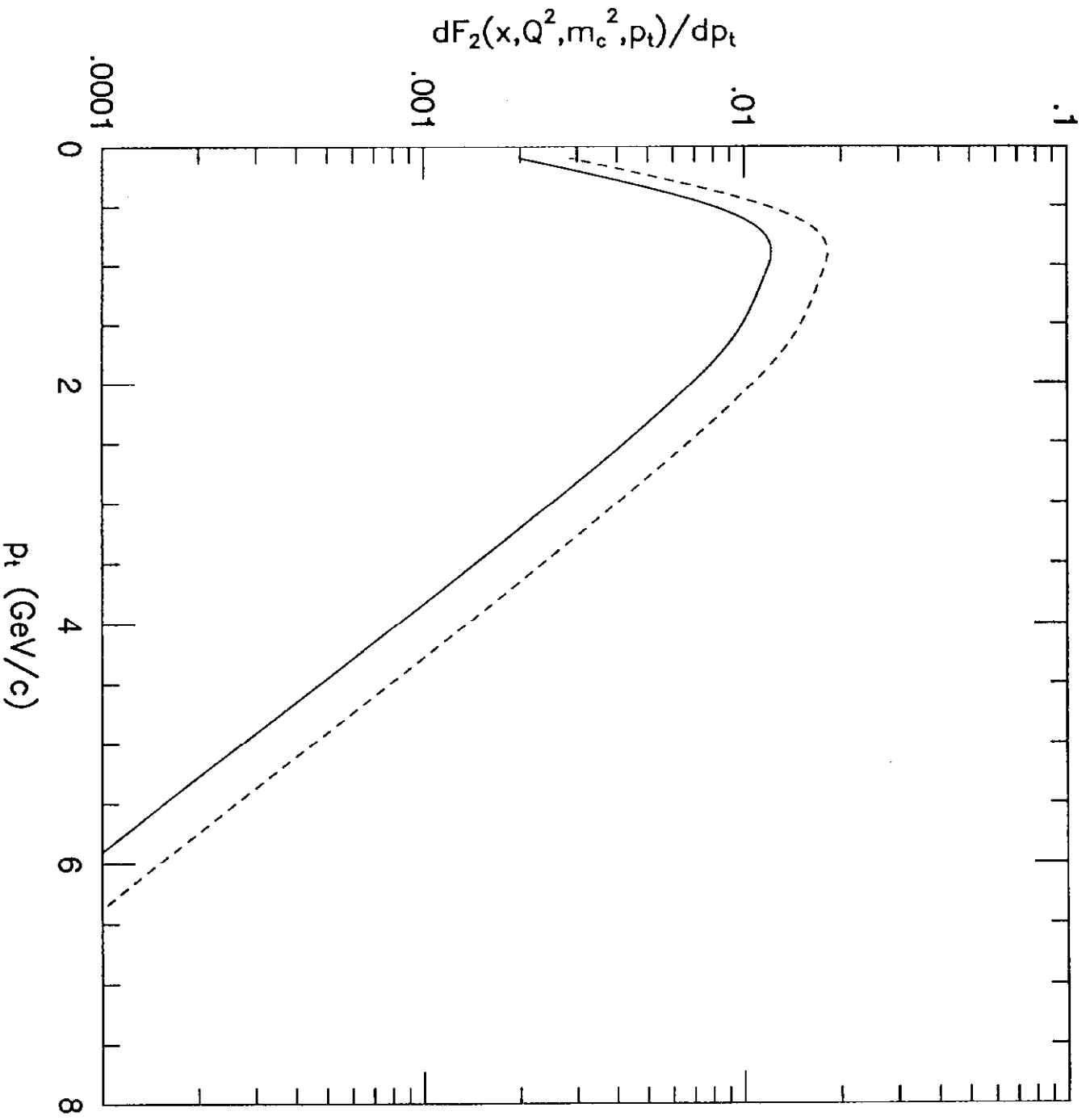


Fig. 2

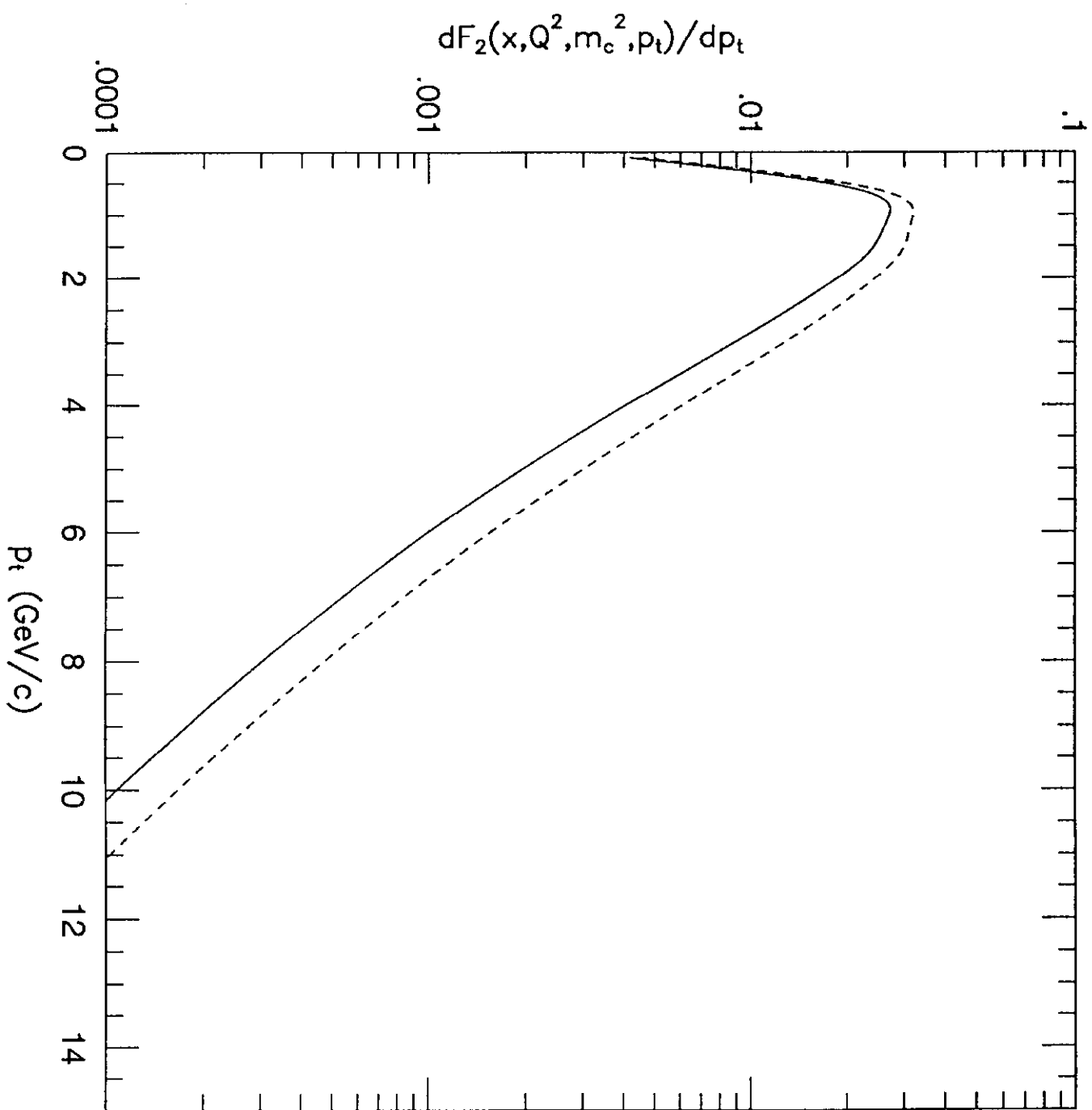


Fig. 3

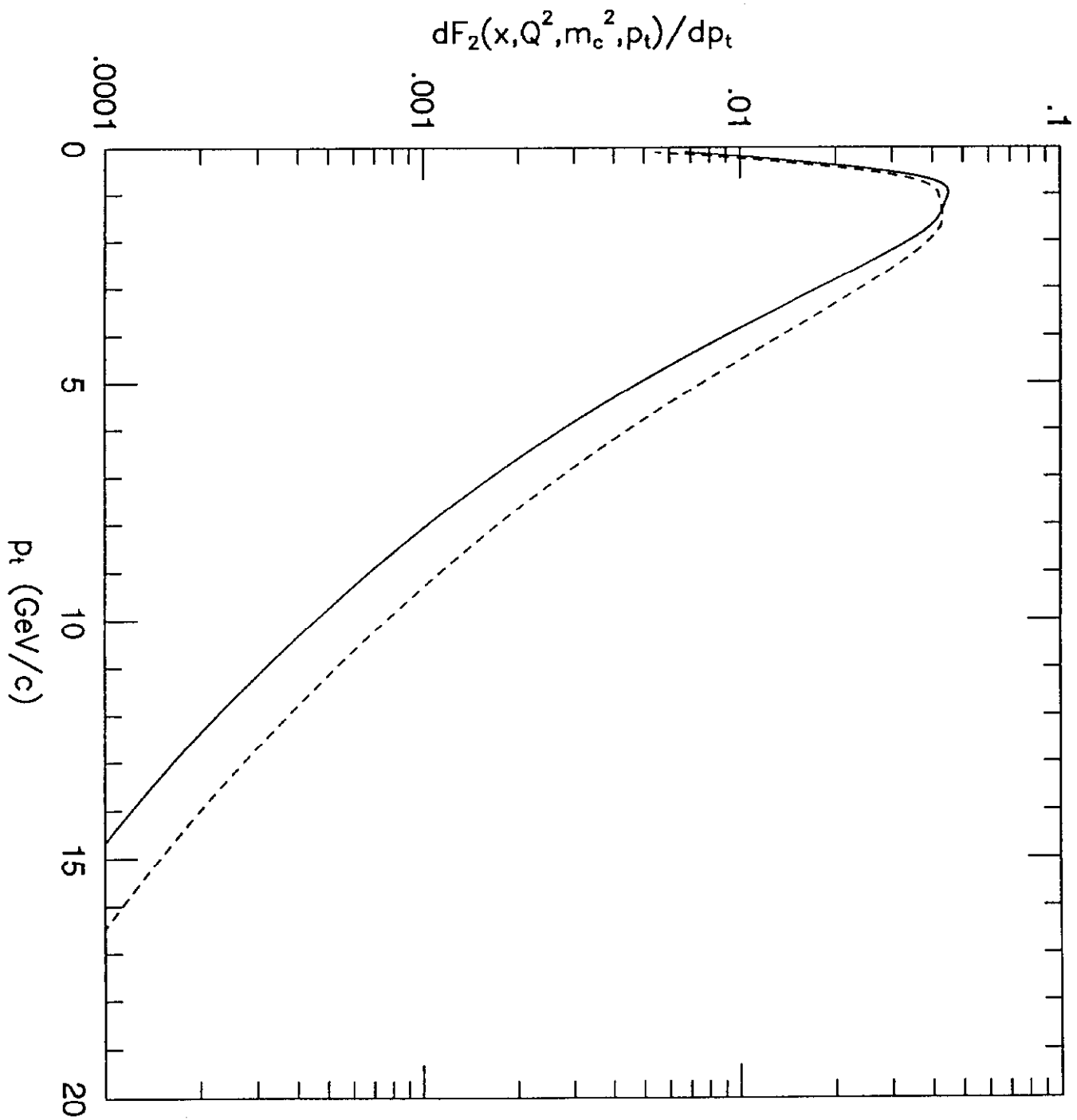


Fig. 4

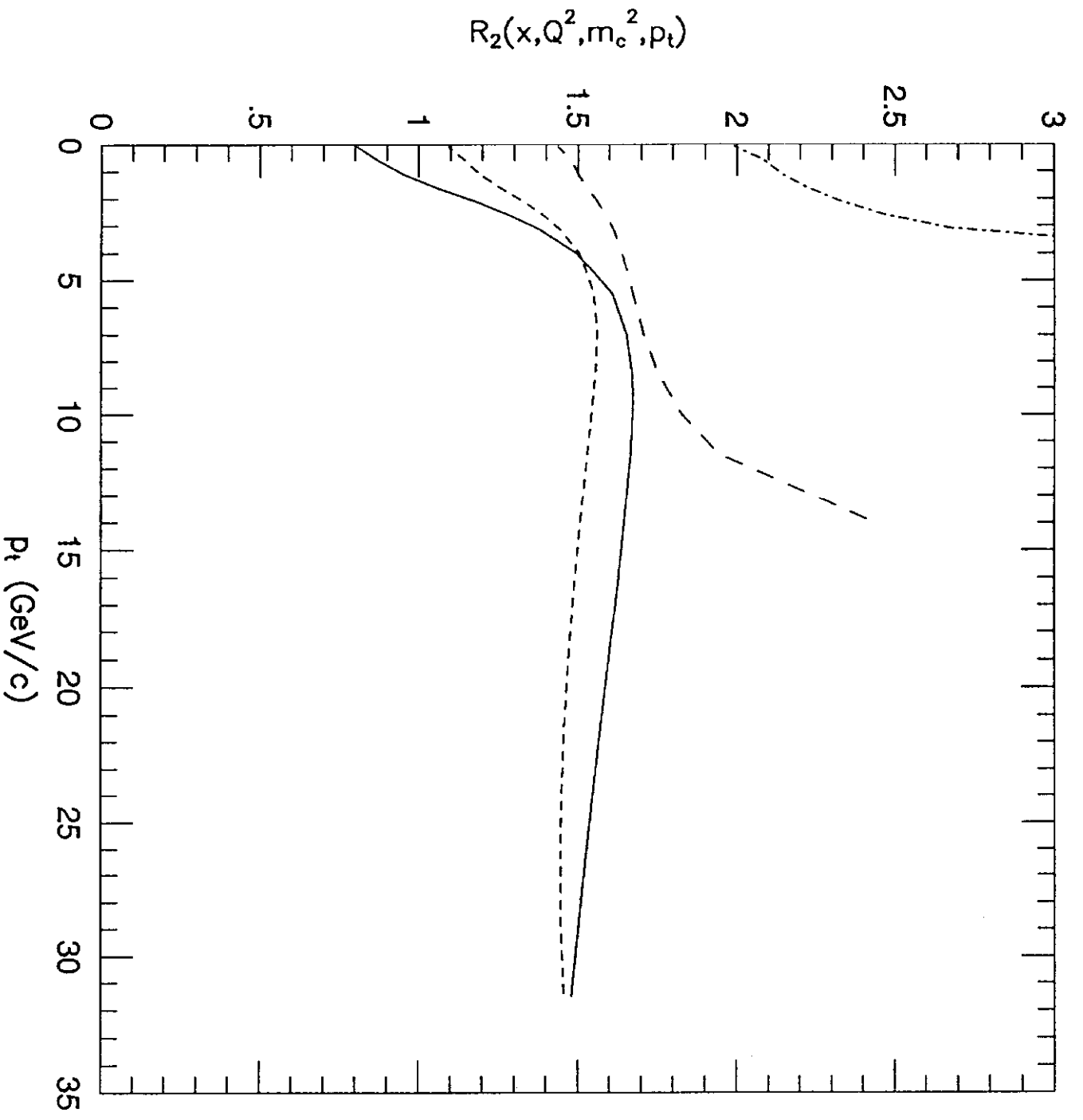


Fig. 5

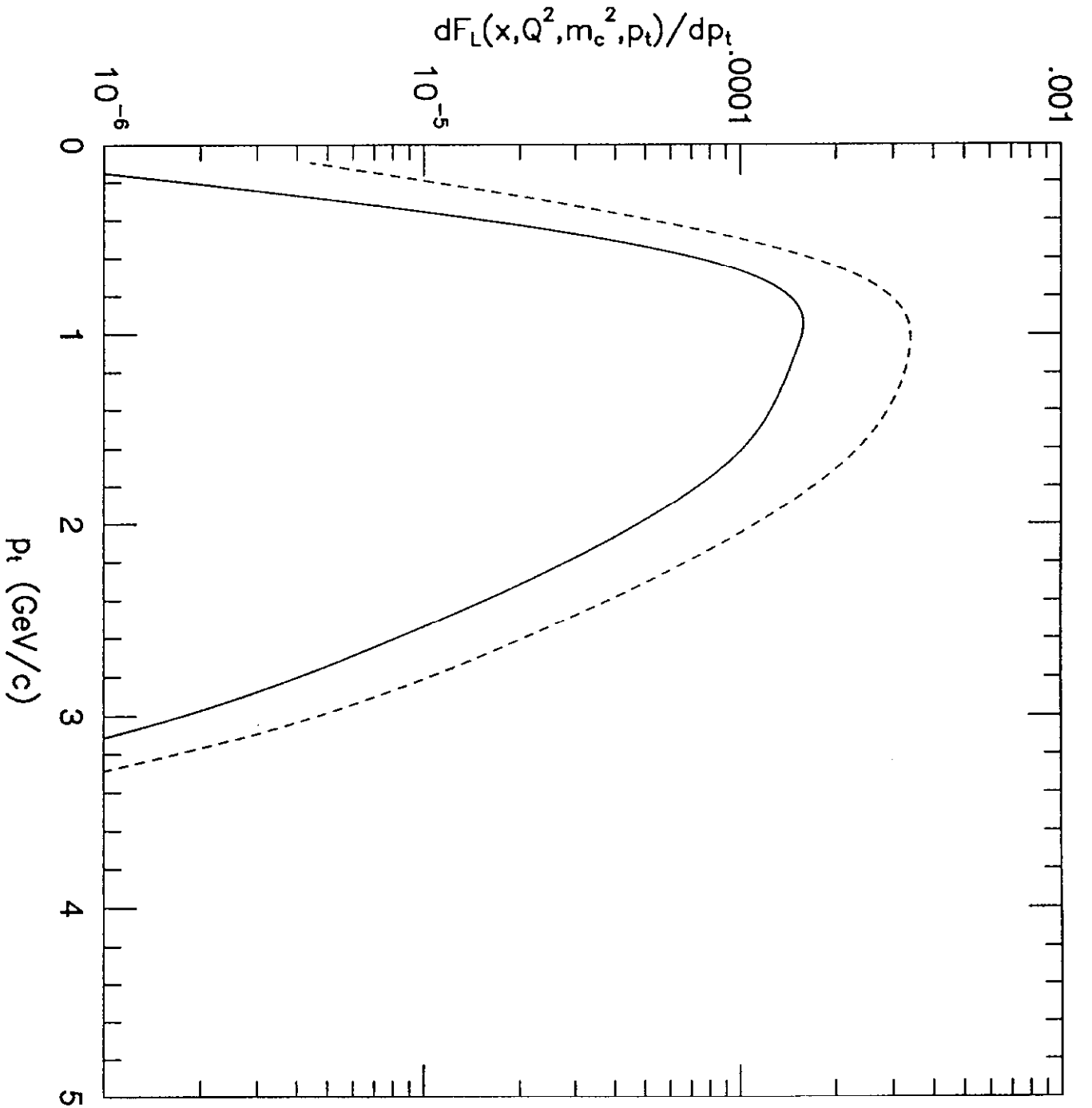


Fig. 6

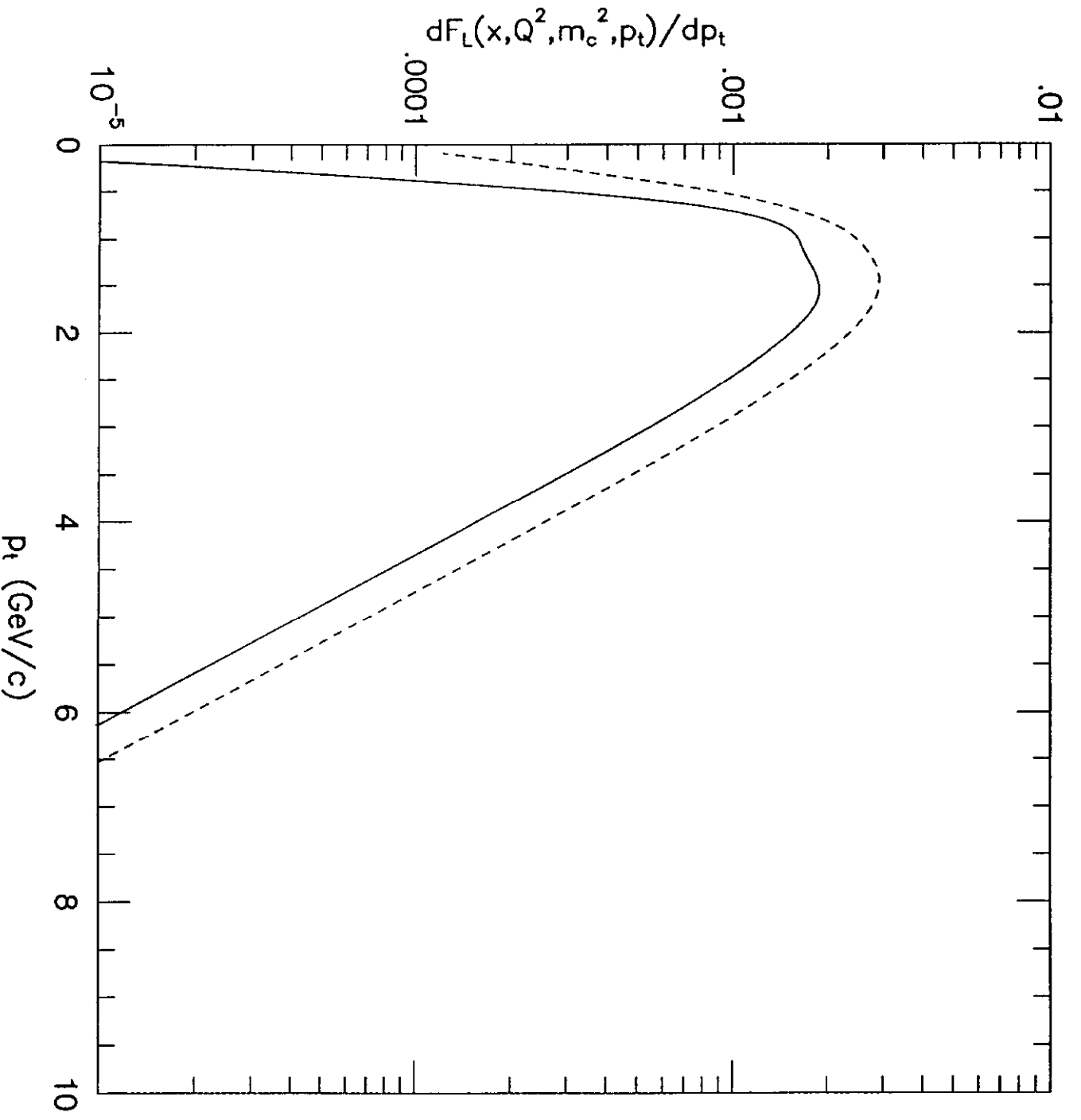


Fig. 7

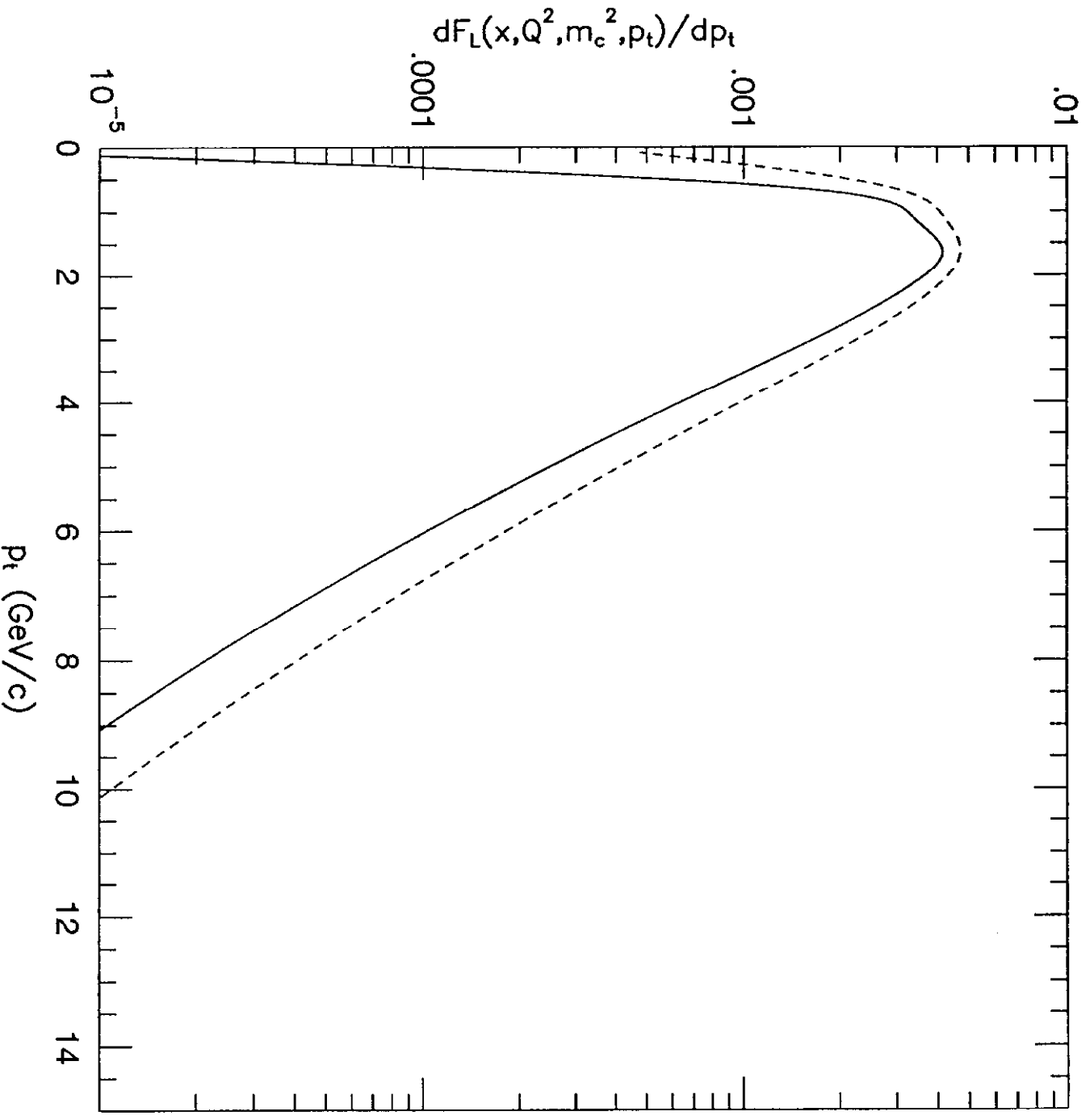


Fig. 8

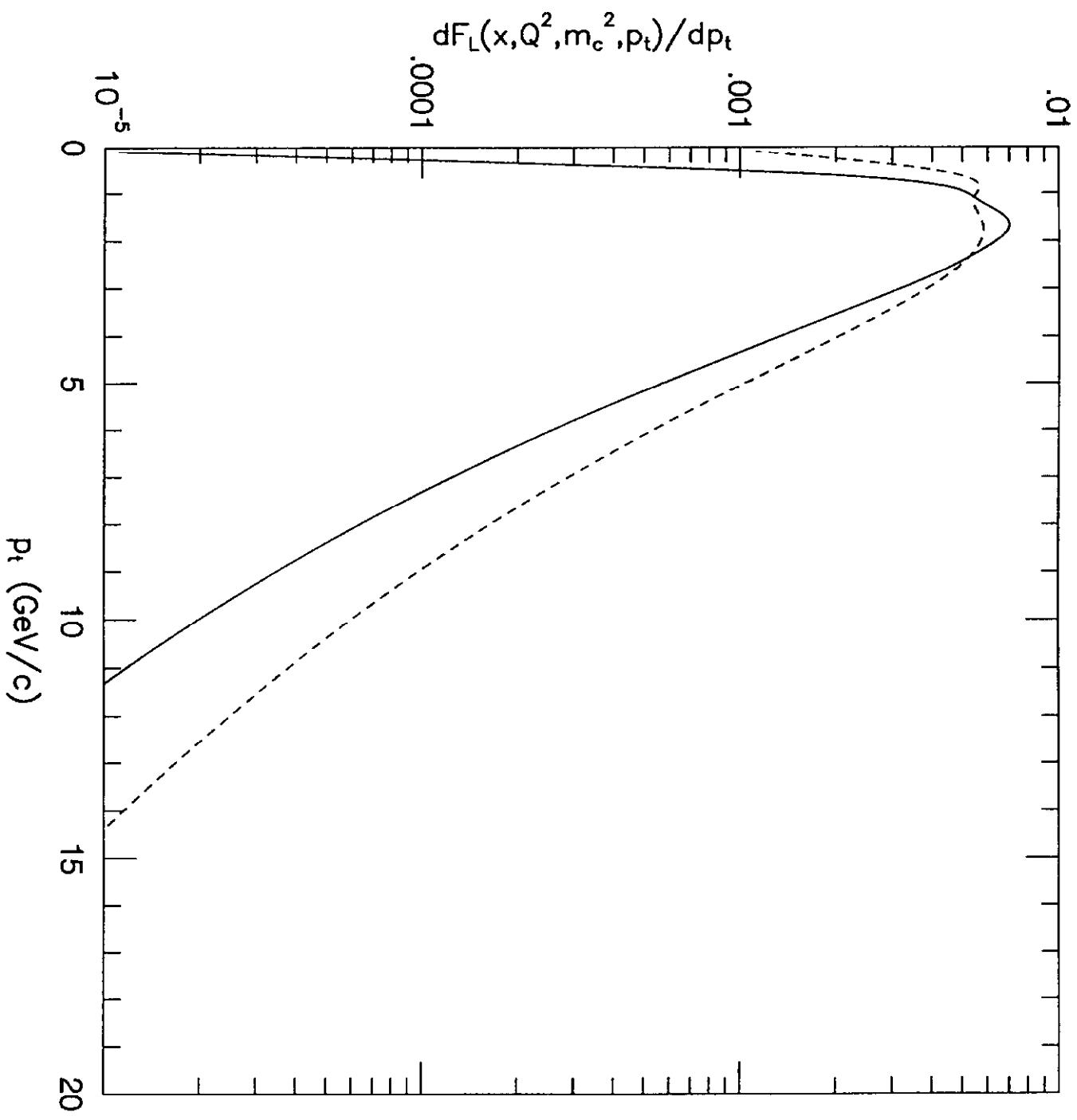


Fig. 9

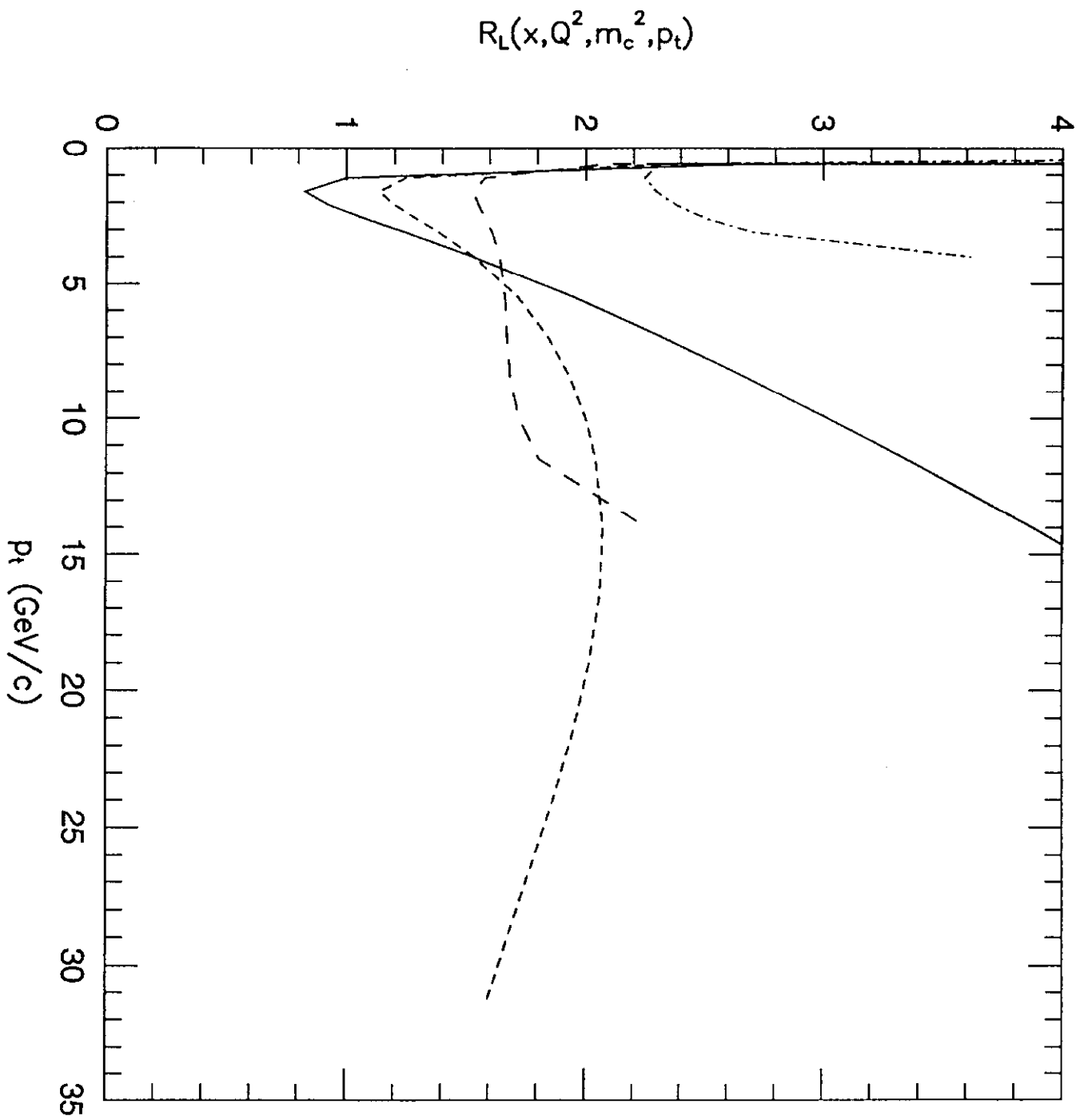


Fig. 10

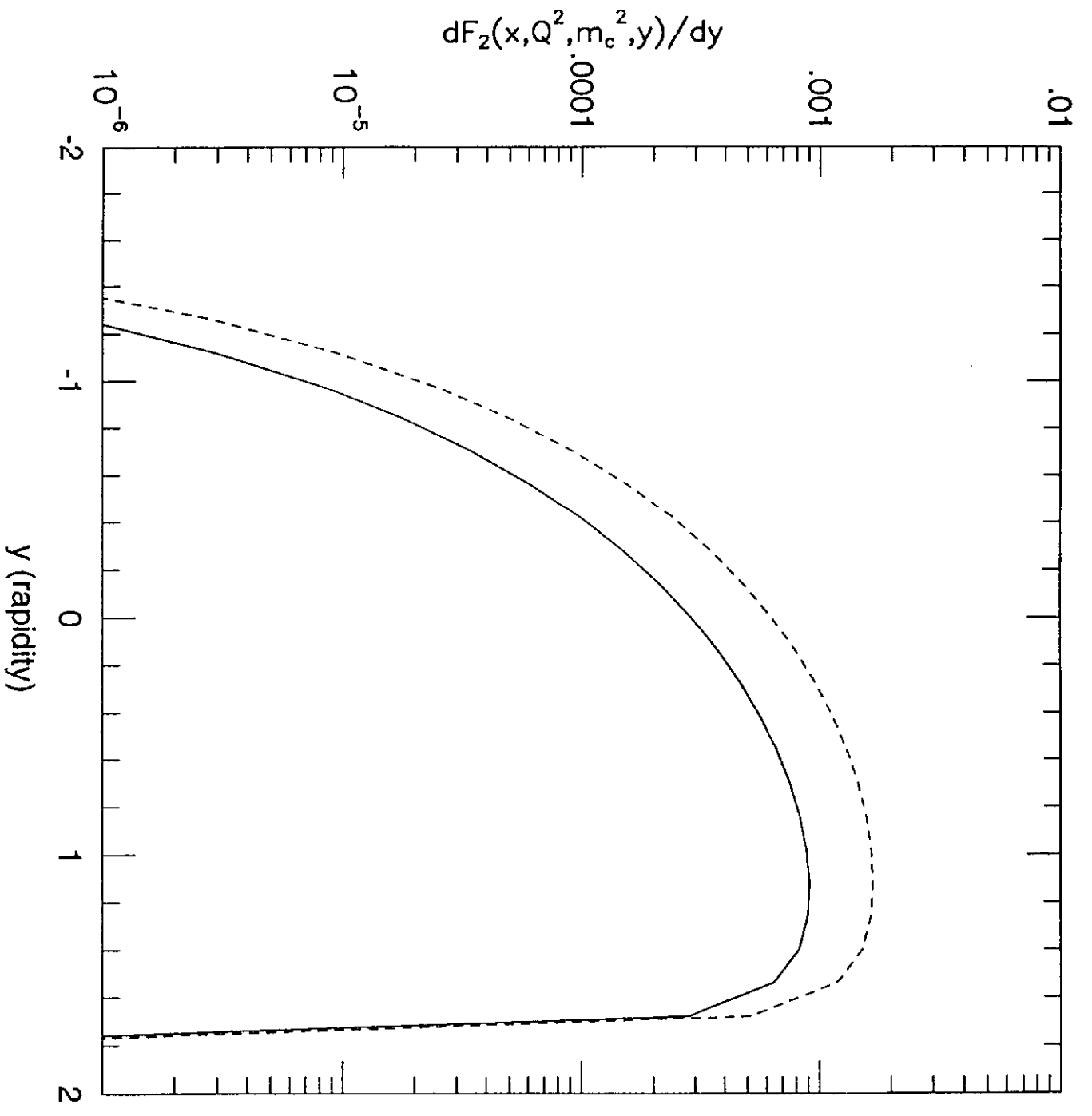


Fig. 11

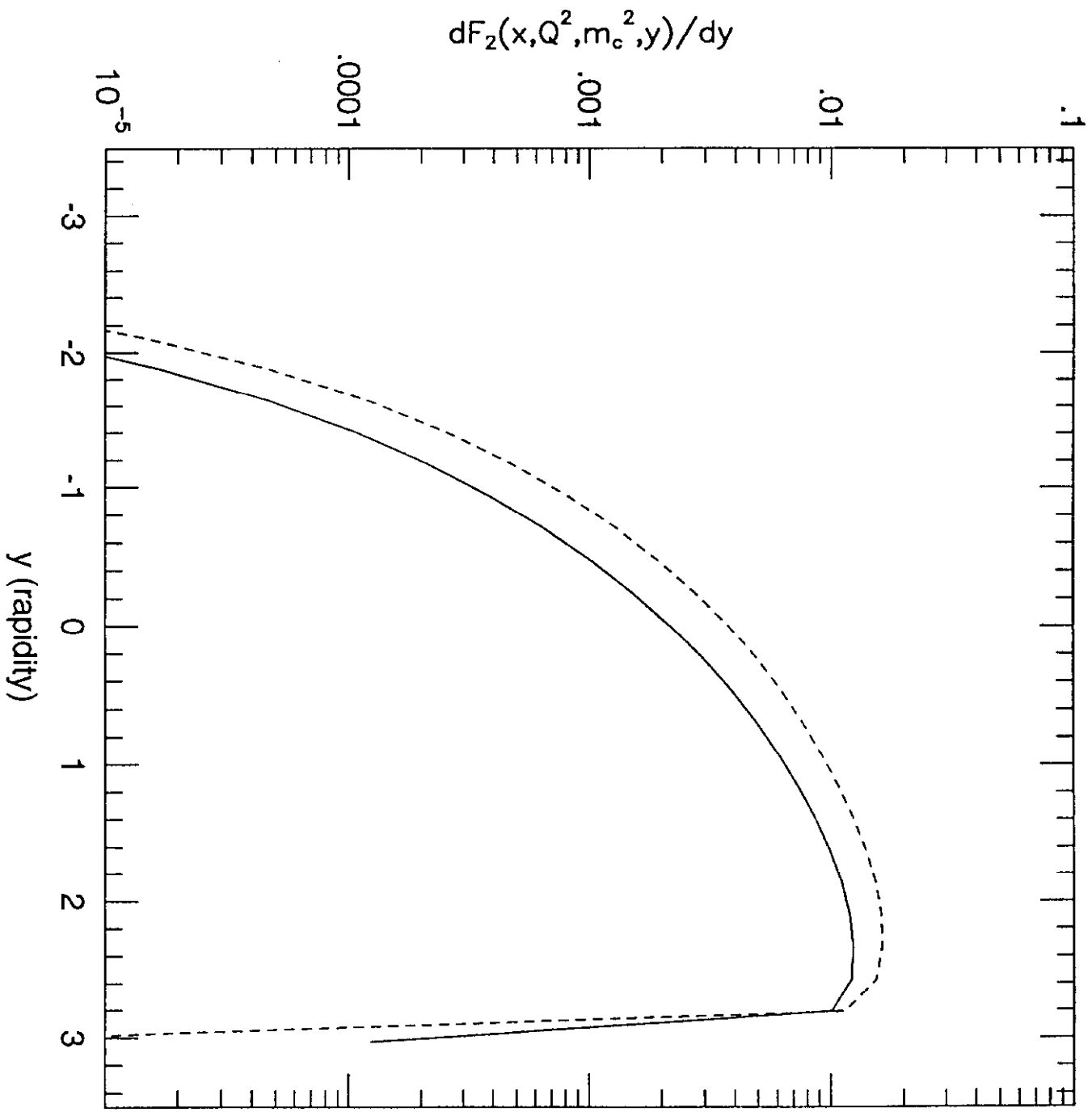


Fig.12

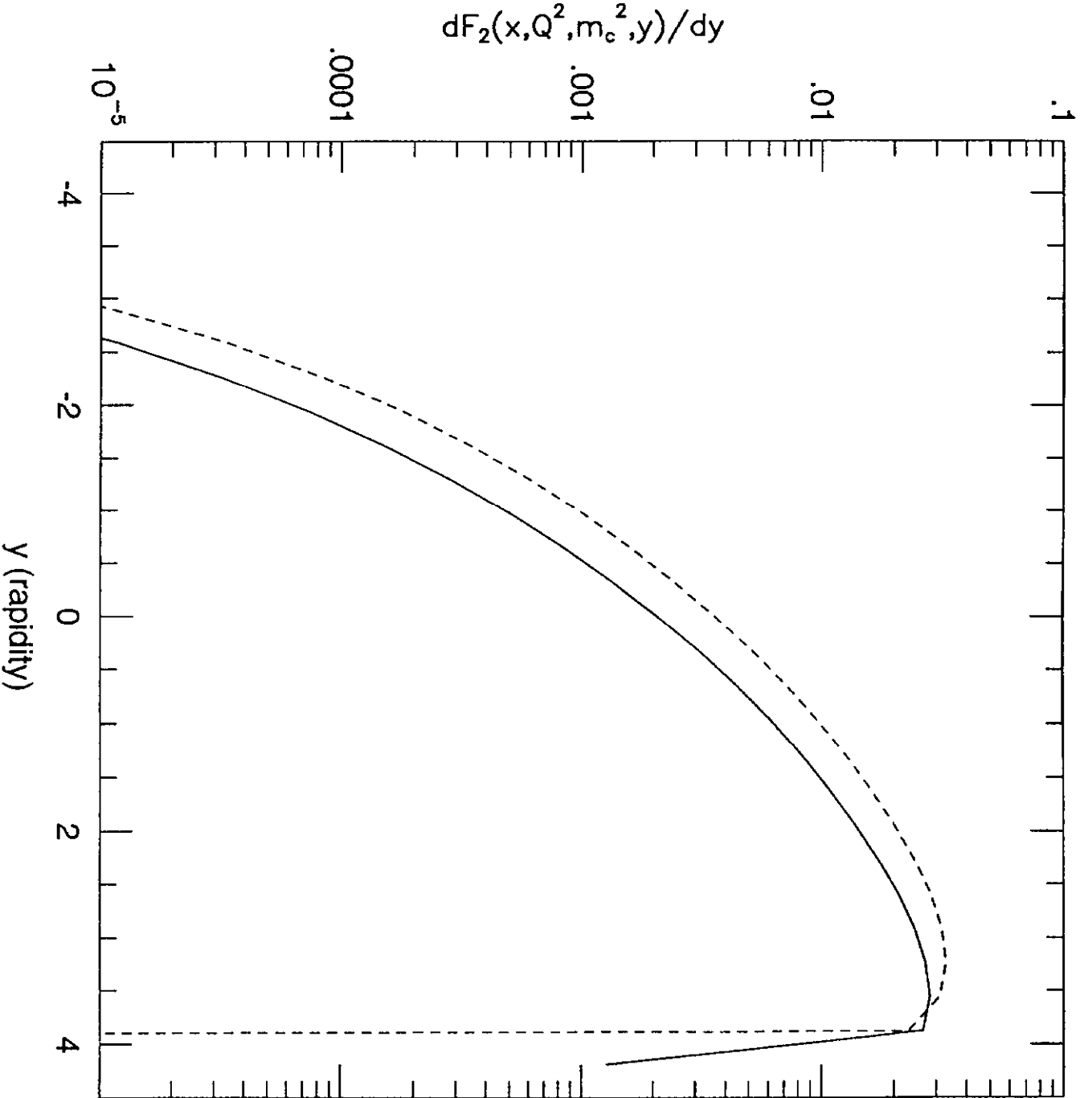


Fig 13

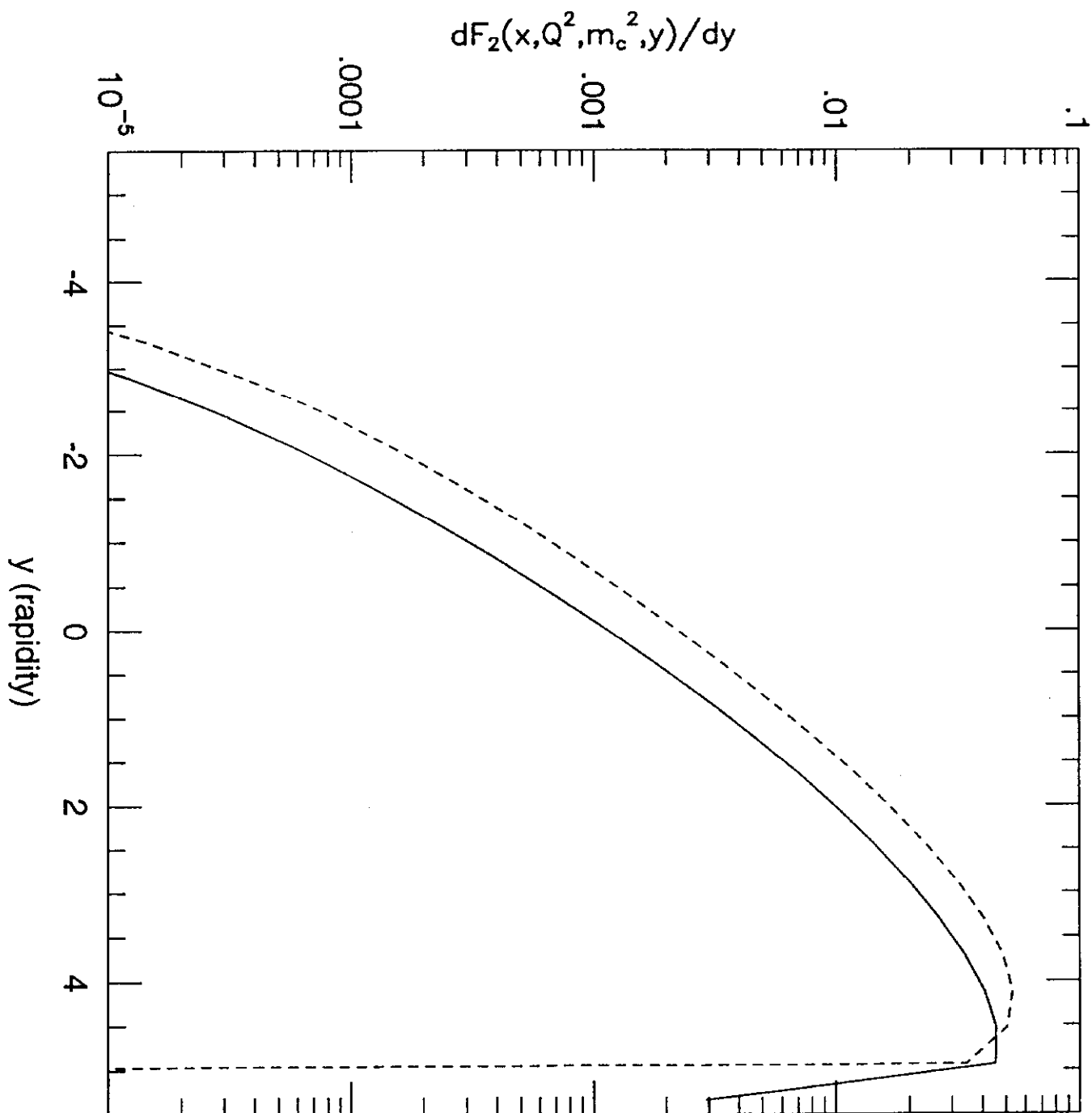


Fig. 14

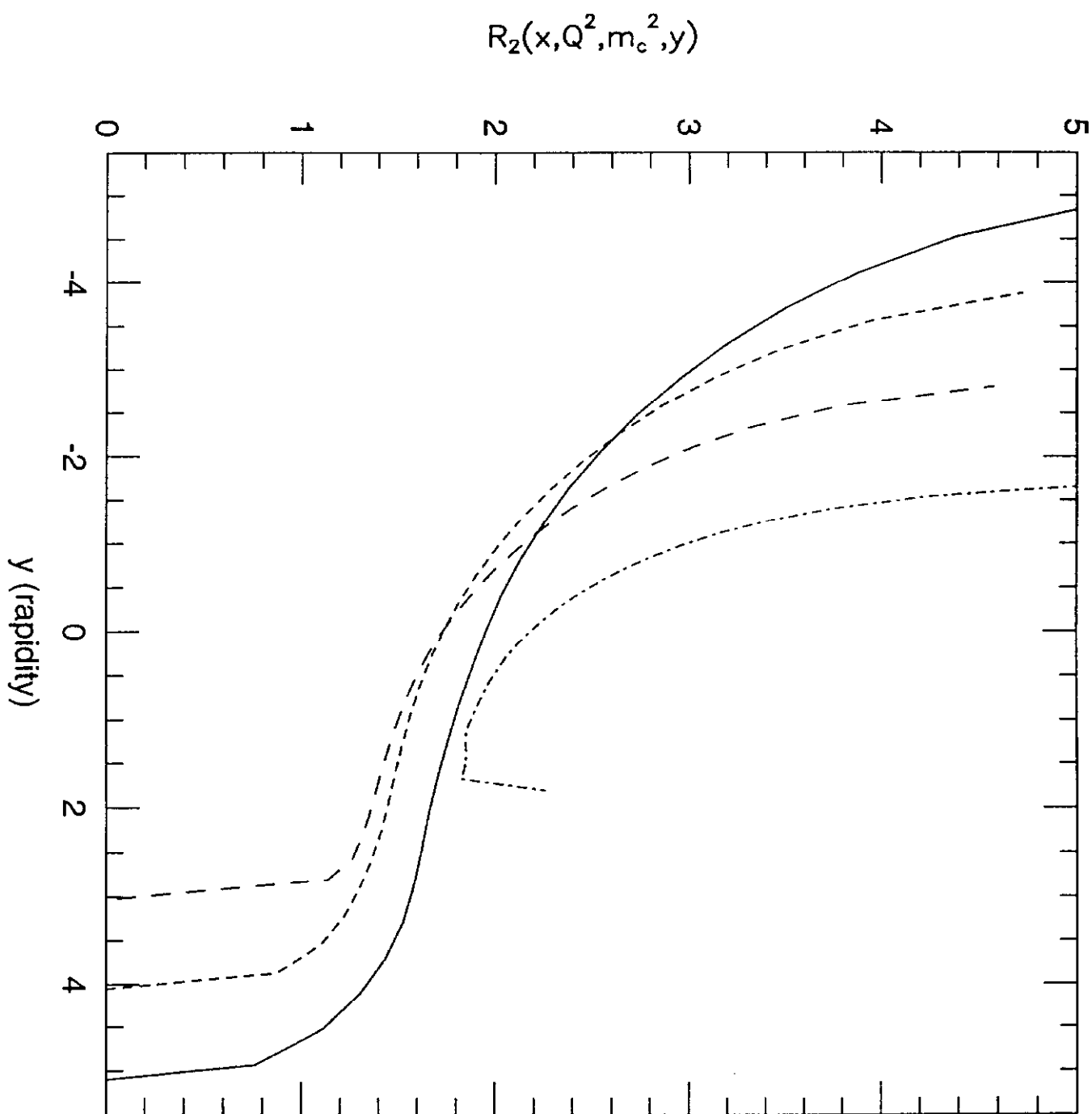


Fig. 15

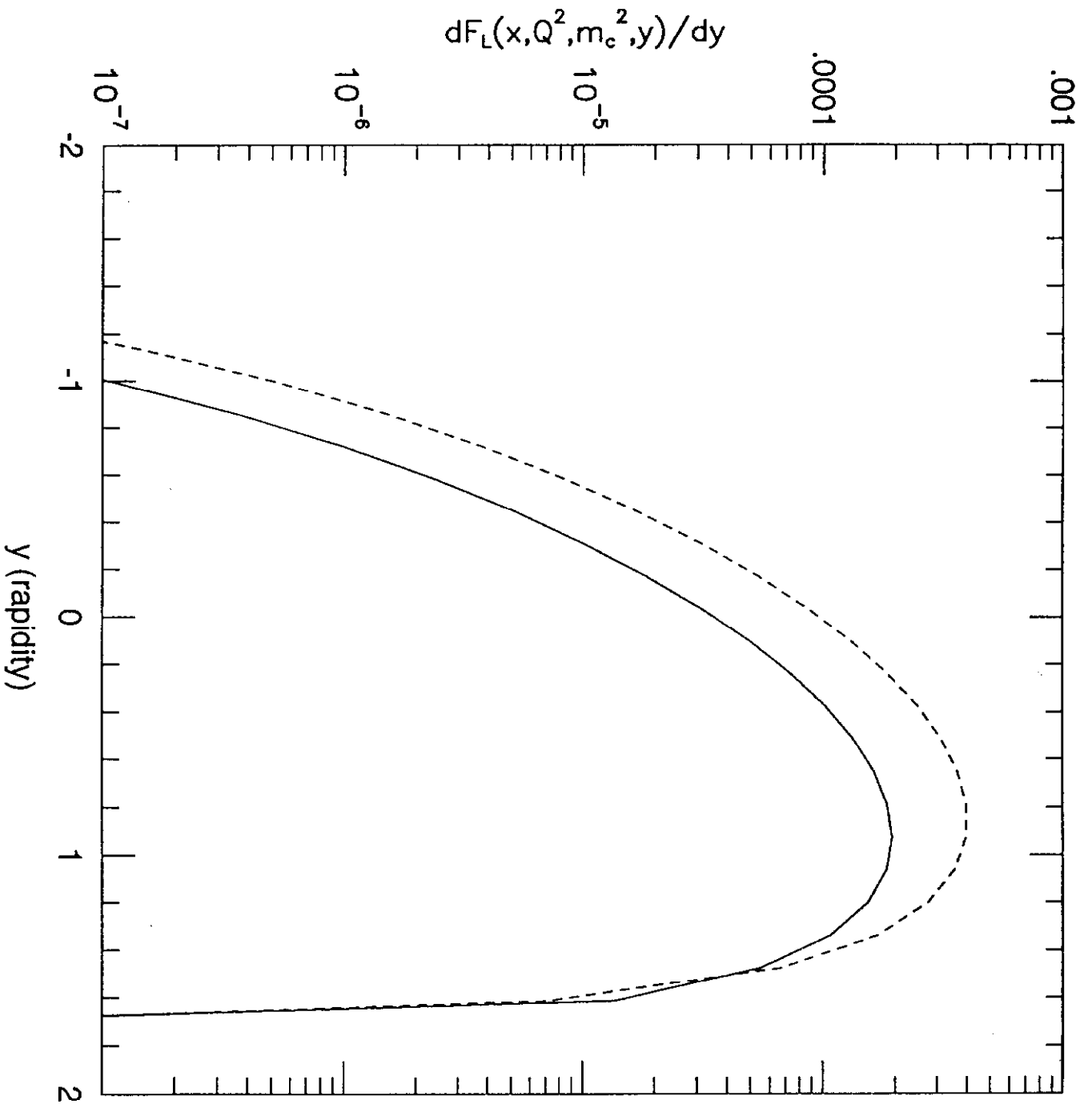


Fig. 16

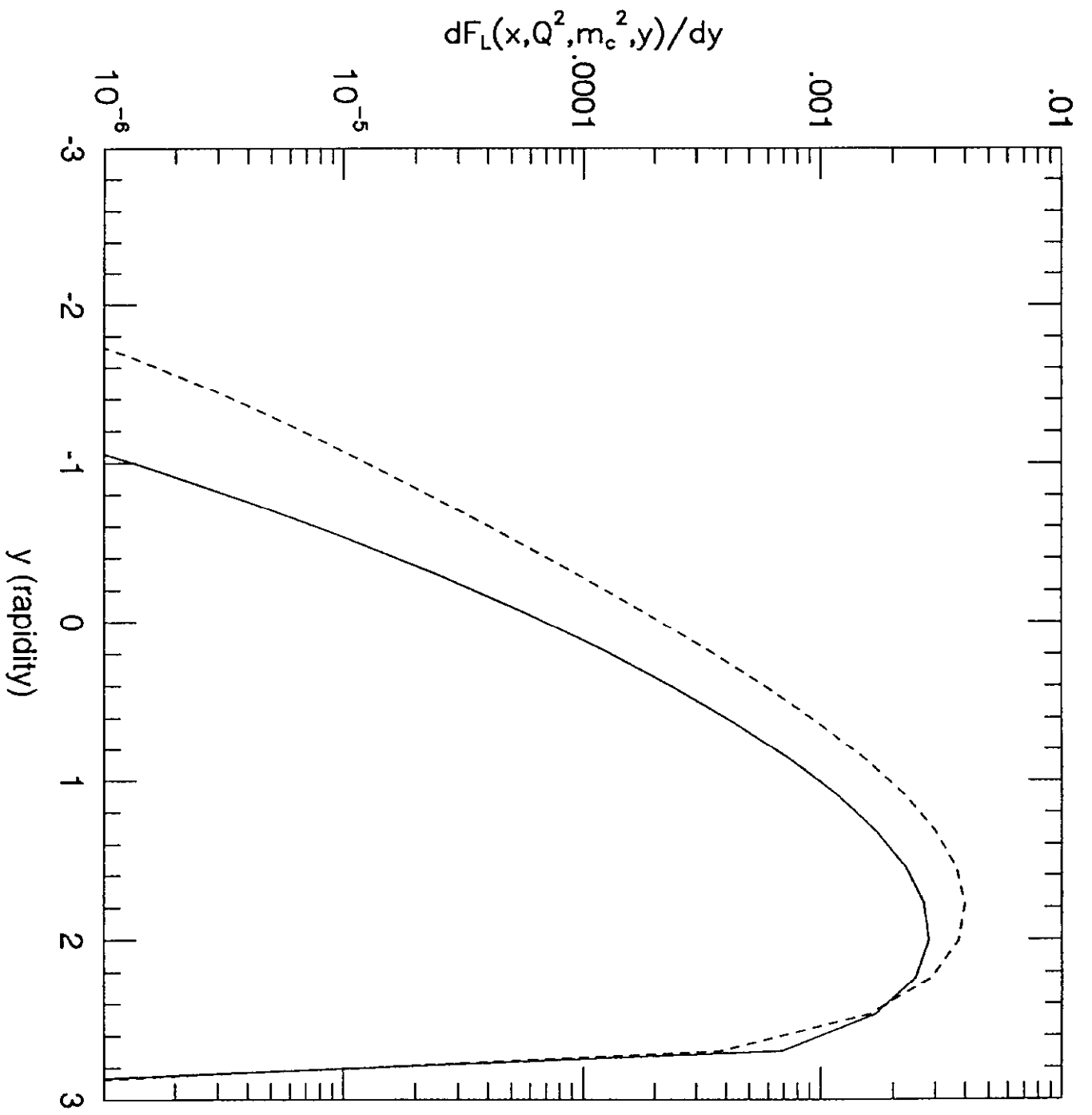


Fig 17

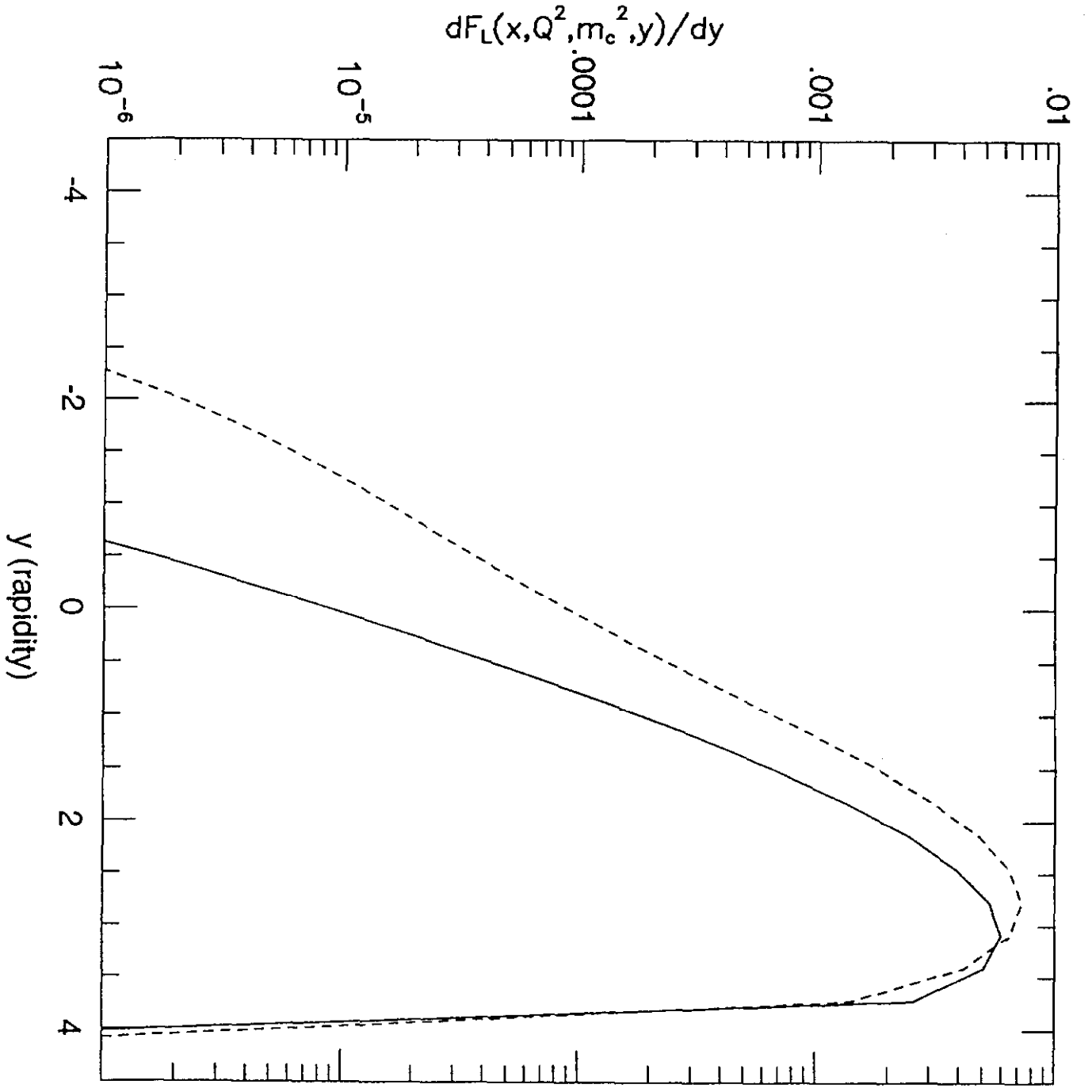


Fig. 18

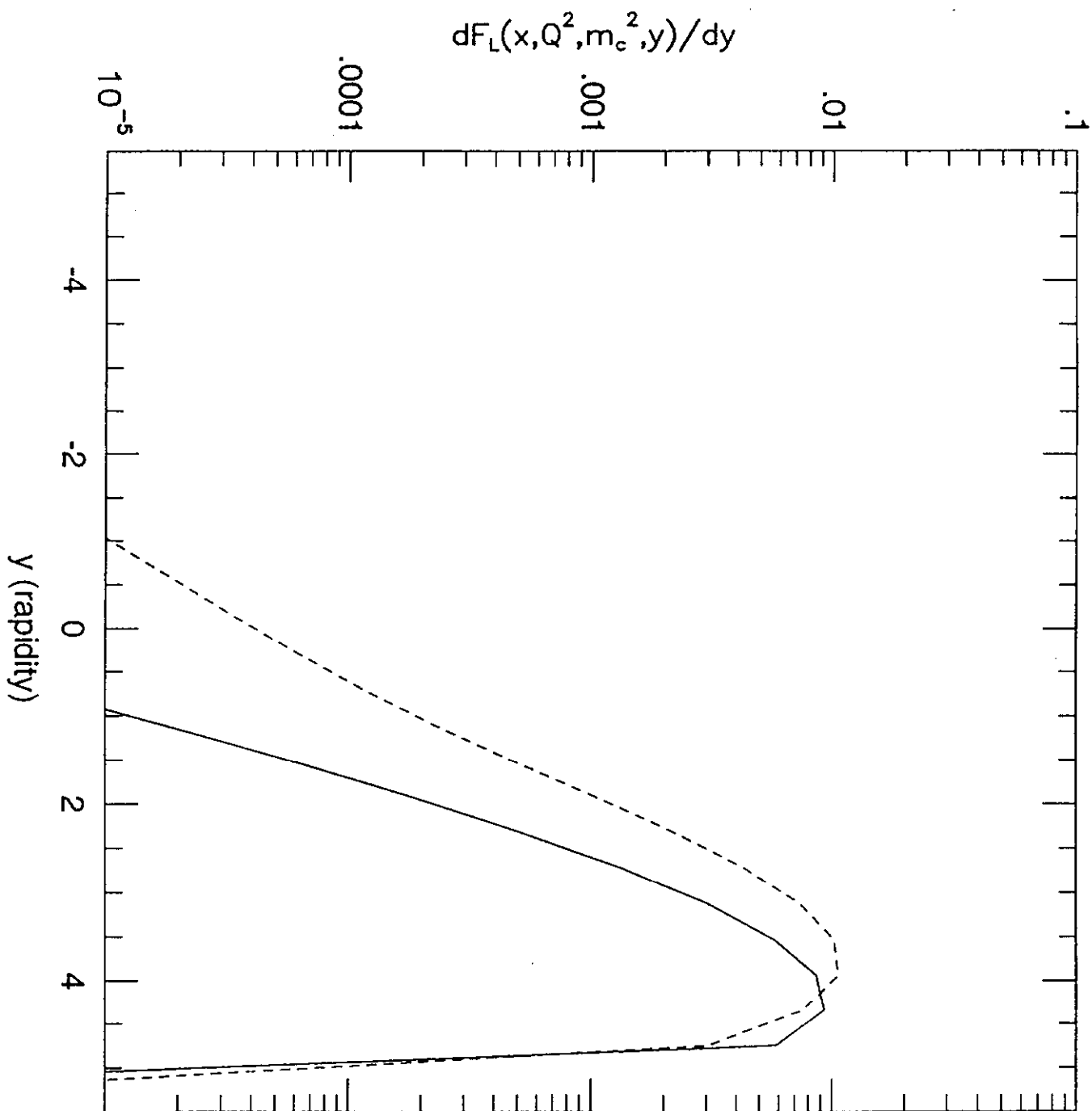


Fig. 19

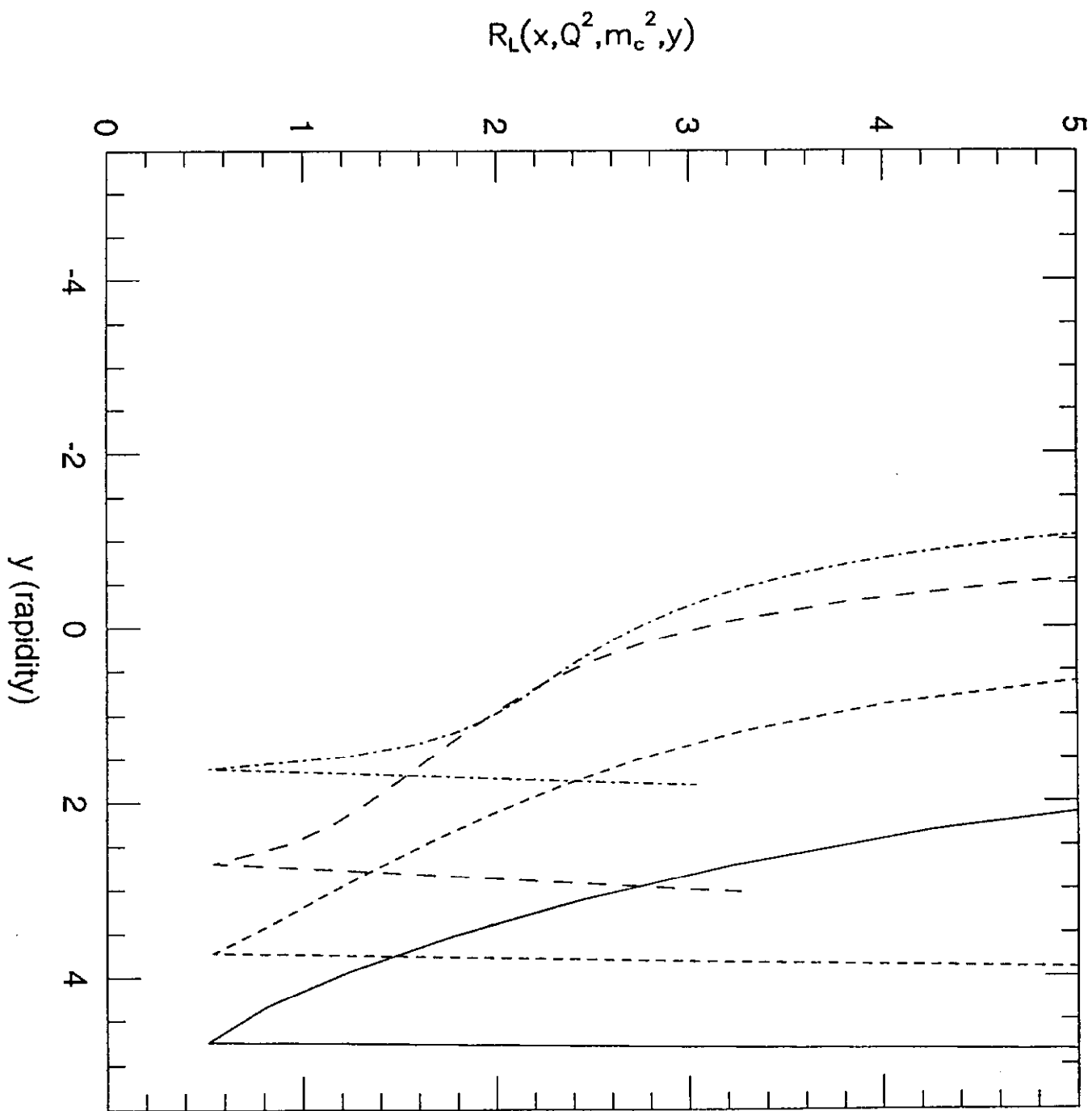


Fig. 20